Inorg. Chem. **2007**, *46*, 9790–9807

Phosphine-Substituted Dithiolene Complexes as Ligands: Communication between Ruthenium(II) Centers Through a Dimolybdenum Bis(dithiolene) Core

Harry Adams,[†] Michael J. Morris,*[,†] Andrea E. Riddiough,[†] Lesley J. Yellowlees,[‡] and A. B. P. Lever*[,§]

Department of Chemistry, University of Sheffield, Sheffield S3 7HF, U.K., School of Chemistry, University of Edinburgh, West Mains Road, Edinburgh EH9 3JJ, U.K., and Department of Chemistry, York University, CB124, 4700 Keele Street, Toronto, Ontario M3J1P3, Canada

Received June 19, 2007

The reaction of $Mo_2(SCH_2CH_2S)_2Cp_2$ (**1**; Cp = η-C_5H_5) with an excess of an alkyne in refluxing dichloromethane affords the bis(dithiolene) complexes $Mo_2(\mu$-$SCR^1{=}CR^2S)_2Cp_2$ (**2a**, $R^1 = R^2 = CO_2Me$; **2b**, $R^1 = R^2 =$ Ph; **2c**, $R^1 = H$, $R^2 = CO_2Me$) whereas with 1 equiv of alkyne at room temperature the mixed dithiolene–dithiolate species $Mo_2(\mu$-$SCR^1{=}CR^2S)(\mu$-$SCH_2CH_2S)Cp_2$ (**3a**, $R^1 = R^2 = CO_2Me$; **3b**, $R^1 = R^2 =$ Ph) are formed. The remaining dithiolate ligand in **3** can then be converted into a different dithiolene by reaction with a second alkyne. Applying this methodology, we have used bis(diphenylphosphino)acetylene to prepare the first examples of complexes containing phosphine-substituted dithiolene ligands: $Mo_2\{\mu$-$SC(CO_2Me){=}C(CO_2Me)S\}\{\mu$-$SC(PPh_2){=}C(PPh_2)S\}$-$Cp_2$ (**2g**) and $Mo_2\{\mu$-$SC(PPh_2){=}C(PPh_2)S\}_2Cp_2$ (**2h**). Tri- and tetrametallic complexes can then be assembled by coordination of these diphosphines to CpRuCl units by reaction with $CpRu(PPh_3)_2Cl$. Electrochemical studies of the Ru(II)/Ru(III) couple in $Mo_2\{\mu$-$SC(PPh_2){=}C(PPh_2)S\}_2Cp_2(RuClCp)_2$ (**4b**) reveals that the two separate ruthenium centers are oxidized electrochemically at different potentials, demonstrating communication between them through the dimolybdenum bis(dithiolene) core. Density functional theory calculations were carried out to explore the electronic structures of these species and to predict and assign their electronic spectra.

Introduction

Complexes containing the dithiolene (1,2-enedithiolate) ligand have been the subject of much interest since the mid-1960s when a major research effort, particularly by the groups of Schrauzer, Holm, and McCleverty, led to the discovery of synthetic routes to dithiolene complexes of most of the transition metals.[1] At the time, this interest was driven by three important properties of the dithiolene ligand: its redox activity, its pseudo-aromaticity, and its propensity for stabilizing unusual coordination geometries. The ligand itself was considered able to bear a formal charge of between −2 and 0 due to the presence of dithiolate and dithioketone resonance forms. Since then, dithiolene complexes have been employed in a variety of applications such as conducting and superconducting coordination compounds (particularly those involving the dmit ligand, $C_3S_5^{2-}$), nonlinear optical materials, and liquid crystals.[2] More recently, nickel dithiolenes have received renewed attention as possible agents for the separation of olefins from gas streams.[3] In the case of molybdenum and tungsten dithiolene complexes, added impetus has been given to their study by their involvement in biological systems, namely, the active sites of oxotransferase enzymes.[4]

Heteroleptic dithiolene complexes containing cyclopentadienyl ligands constitute an important subgroup of compounds, particularly for Mo and W.[5] Research in our

* To whom correspondence should be addressed. E-mail: M.Morris@sheffield.ac.uk. (M.J.M.), blever@yorku.ca (A.B.P.L.). Tel: 0114 2229363. Fax: 0114 2229346.
[†] University of Sheffield.
[‡] University of Edinburgh.
[§] York University.

(1) (a) McCleverty, J. A. *Prog. Inorg. Chem.* **1969**, *10*, 49. (b) Eisenberg, R. *Prog. Inorg. Chem.* **1970**, *12*, 295. (c) Burns, R. P.; McAuliffe, C. A. *Adv. Inorg. Chem. Radiochem.* **1979**, *22*, 303. (d) Mueller-Westerhoff, U. T.; Vance, B. In *Comprehensive Coordination Chemistry*; Wilkinson, G., Gillard, R. D., McCleverty, J. A., Eds.; Pergamon: Oxford, 1987; Vol. 2, Chapter 16.5. (e) Dithiolene Chemistry; Stiefel, E. I., Ed.; *Prog. Inorg. Chem.* **2004**, *52*.

(2) (a) Mueller-Westerhoff, U. T.; Vance, B.; Yoon, D. I. *Tetrahedron* **1991**, *47*, 909. (b) Robertson, N.; Cronin, L. *Coord. Chem. Rev.* **2002**, *227*, 93. (c) Fourmigué, M. *Acc. Chem. Res.* **2004**, *37*, 179.

(3) Wang, K.; Stiefel, E. I. *Science* **2001**, *291*, 106.

(4) (a) Hille, R. *Chem. Rev.* **1996**, *96*, 2757. (b) Johnson, M. K.; Rees, D. C.; Adams, M. W. W. *Chem. Rev.* **1996**, *96*, 2817.

10.1021/ic701201x CCC: $37.00
Published on Web 10/02/2007

laboratory is focused on discovering new synthetic routes to both mono- and dinuclear complexes of this type, exemplified by the recent synthesis of $CpMo(S_2C_2Ph_2)_2$ and $Mo_2\{\mu\text{-}C_2(CO_2Me)_2\}(\mu\text{-}S_2C_2Ph_2)_2Cp_2$ (Cp = η-C_5H_5) by means of dithiolene transfer reactions[6] and our development of two complementary routes to the dinuclear Mo(V) compounds $[Mo_2S(\mu\text{-}S)_2(SCR^1{=}CR^2S)Cp_2]$ containing a terminal dithiolene ligand.[7]

In the course of these studies, we became interested in the related Mo(III) complexes $Mo_2(\mu\text{-}SCR^1{=}CR^2S)_2Cp_2$, which contain two bridging dithiolene ligands. These have been known since King prepared the first example ($R^1 = R^2 = CF_3$) by the reaction of $Mo_2(CO)_6Cp_2$ with the dithiete $S_2C_2(CF_3)_2$;[8] further clarification of this reaction, together with the X-ray structure of the product, was later provided by Miessler and co-workers.[9] Convenient access to a wider range of compounds of this type, including the first examples containing unsymmetrical dithiolenes ($R^1 \neq R^2$), became available by exchange of the alkene portion of the dithiolate ligands in $Mo_2(SCH_2CHRS)_2Cp_2$ (R = H, Me) with the alkynes $R^1C{\equiv}CR^2$ ($R^1 = R^2 = H$; R^1 = H or Me, R^2 = Ph).[10] The crystal structure of the parent complex ($R^1 = R^2 = H$) was reported separately.[11] More recently, Sugimori has shown that low yields of the complex with $R^1 = R^2 = CO_2Me$ can be obtained (together with several other carbonyl-containing dithiolene complexes) by the reaction of $Mo_2(CO)_6Cp_2$ with sulfur and dimethyl acetylenedicarboxylate (DMAD, $MeO_2CC{\equiv}CCO_2Me$).[12] This is reminiscent of the original King reaction in that a dithiete may possibly be an intermediate.[13]

Here, we present further developments in the chemistry of these complexes, including (i) a general preparation of those containing two different bridging dithiolene ligands (whereas complexes containing two or more dithiolene ligands are relatively common, those containing two *different* dithiolene ligands are very rare); (ii) complexes containing the first examples of phosphine-substituted dithiolene ligands; (iii) the coordination of additional metal fragments to the phosphine substituents; (iv) the electrochemical characterization of the resulting species which reveals communication between the metal centers across the dimolybdenum core through the dithiolene ligands; and (v) density functional theory (DFT) calculations used to explore the electronic structures of these species and assign their electronic spectra.

Scheme 1. Synthesis of the Bridging Dithiolene Complexes **2** and **3**

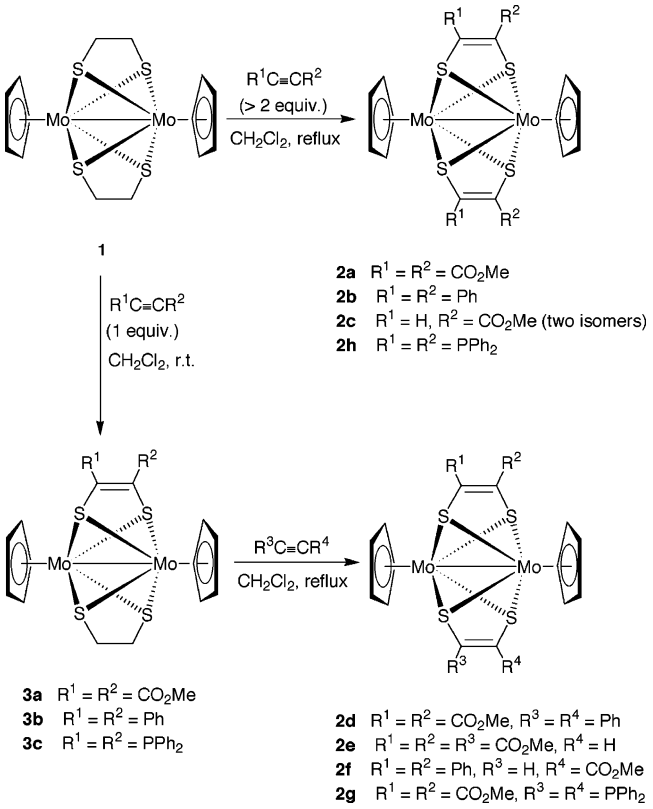

Results and Discussion

Synthetic Studies. We chose to expand the methodology of Dubois,[10] as these reactions occurred under mild conditions and used alkynes as the source of the dithiolene ligands. Treatment of $Mo_2(SCH_2CH_2S)_2Cp_2$ (**1**) with an excess of DMAD or C_2Ph_2 in refluxing dichloromethane for 24−48 h duly provided the symmetrical bis-dithiolene complexes **2a** and **2b** as air-stable brick-red (**2a**) or green-brown (**2b**) solids in yields of 57 and 64%, respectively (Scheme 1). Their relative insolubility prevented the acquisition of ^{13}C NMR spectra, but characterization by ^1H NMR spectra, mass spectra, and elemental analysis proved straightforward. The data obtained for **2a** agreed with those recently reported by Sugimori.[12] The reaction of **1** with methyl propiolate under similar conditions afforded the analogous complex $Mo_2\{\mu\text{-}SCH{=}C(CO_2Me)S\}Cp_2$ (**2c**) (62%) as two separable isomers, cis and trans, depending on the relative orientation of the two unsymmetrical dithiolene ligands. The presence of isomers was not observed in the previous bis-dithiolene complexes of this type prepared from the unsymmetrical alkynes PhC≡CH and PhC≡CMe.[10] The ^1H NMR spectrum of the cis isomer exhibited a peak at δ 7.78 for the CH of the dithiolene, with the corresponding peak for the trans isomer occurring at δ 7.80. These figures are typical for bridging dithiolene ligands, whereas protons attached to terminal dithiolenes appear at lower field, e.g., δ 9.41 for $[Mo_2S(\mu\text{-}S)_2\{SCH{=}C(CO_2Me)S\}Cp_2]$.[6] Only the cis isomer was sufficiently soluble to permit the recording of a ^{13}C NMR spectrum, in which both signals due to the dithiolene carbon atoms appeared in the region of 160 ppm. The stereochem-

(5) Fourmigué, M. *Coord. Chem. Rev.* **1998**, *178−180*, 823.
(6) (a) Adams, H.; Gardner, H. C.; McRoy, R. A.; Morris, M. J.; Motley, J. C.; Torker, S. *Inorg. Chem.* **2006**, *45*, 10967. (b) Adams, H.; Morris, M. J.; Morris, S. A.; Motley, J. C. *J. Organomet. Chem.* **2004**, *689*, 522.
(7) Abbott, A.; Bancroft, M. N.; Morris, M. J.; Hogarth, G.; Redmond, S. P. *Chem. Commun.* **1998**, 389.
(8) King, R. B. *J. Am. Chem. Soc.* **1963**, *85*, 1587.
(9) Roesselet, K.; Doan, K. E.; Johnson, S. D.; Nicholls, P.; Miessler, G. L.; Kroeker, R.; Wheeler, S. H. *Organometallics* **1987**, *6*, 480.
(10) Rakowski Dubois, M.; Haltiwanger, R. C.; Miller, D. J.; Glatzmeier, G. *J. Am. Chem. Soc.* **1979**, *101*, 5245.
(11) Miller, W. K.; Haltiwanger, R. C.; VanDerVeer, M. C.; Rakowski Dubois, M. *Inorg. Chem.* **1983**, *22*, 2973.
(12) Sugiyama, T.; Yamanaka, T.; Shibuya, M.; Nakase, R.; Kajitani, M.; Akiyama, T.; Sugimori, A. *Chem. Lett.* **1998**, 501.
(13) For the isolation of this dithiete by a different method, see Shimizu, T.; Murakami, H.; Kobayashi, Y.; Iwata, K.; Kamigata, N. *J. Org. Chem.* **1998**, *63*, 8192.

istry of the trans isomer was confirmed by an X-ray structure determination, reported below.

In order to control the degree of functionalization of the dithiolene ligands completely, we wanted to establish reliable syntheses of complexes containing two different dithiolene ligands. Dubois and co-workers had briefly reported that the reaction of **1** with 1 equiv of phenylacetylene in CH_2Cl_2 at room temperature afforded the mixed dithiolene−dithiolate complex $Mo_2(\mu\text{-SCH=CPhS})(\mu\text{-SCH}_2\text{CH}_2\text{S})Cp_2$ in 25% yield.[14] This proved to be a general method: treatment of **1** with 1 equiv of DMAD or C_2Ph_2 under these conditions gave the mixed complexes $Mo_2(\mu\text{-SCR}^1\text{=CR}^2\text{S})(\mu\text{-SCH}_2\text{CH}_2\text{S})Cp_2$ (**3a**, $R^1 = R^2 = CO_2Me$; **3b**, $R^1 = R^2 = Ph$) in moderate yields (44 and 20%, respectively). These green compounds are distinctly more soluble in organic solvents than the bis-dithiolene complexes **2**, so much so that recrystallization of **3a** proved difficult. Their ^1H NMR spectra showed a singlet for the remaining CH_2 groups, together with appropriate signals for R^1 and R^2, and the ^{13}C spectra contained peaks due to dithiolene (ca. 160 ppm) and dithiolate (ca. 35 ppm) carbons.

The alkene portion of the remaining dithiolate ligand in these complexes is also readily replaced by alkynes.[15] Thus, treatment of **3a** with diphenylacetylene or methyl propiolate in refluxing dichloromethane afforded the yellow mixed bis-dithiolene complexes $Mo_2\{\mu\text{-SC(CO}_2\text{Me)=C(CO}_2\text{Me)S}\}(\mu\text{-SCPh=CPhS})Cp_2$ (**2d**) and $Mo_2\{\mu\text{-SC(CO}_2\text{Me)=C(CO}_2\text{Me)S}\}\{\mu\text{-SCH=C(CO}_2\text{Me)S}\}Cp_2$ (**2e**) in yields of 82 and 50%, respectively. There was no evidence for exchange of the existing dithiolene ligands during this process (i.e., no **2a** or **2b** was formed during the first of these reactions). Similarly, treatment of **3b** with methyl propiolate cleanly gave $Mo_2\{\mu\text{-SCH=C(CO}_2\text{Me)S}\}(\mu\text{-SCPh=CPhS})Cp_2$ (**2f**). Presumably, this stepwise procedure could be used to gain access to complexes of type **2** with virtually any combination of substituents, the exact route employed depending on the ease of adding 1 equiv of each particular alkyne.

Phosphine-Substituted Dithiolene Complexes. Phosphine ligands are ubiquitous in organometallic chemistry and catalysis. One of their strengths is the ability to tune their roles by the systematic variation of steric and electronic factors, along with the possibility of building in additional useful properties, e.g., water solubility. Electrochemically active phosphine ligands are a relatively unexplored area, though several recent papers have examined the incorporation of phosphine substituents into the tetrathiafulvalene (TTF) nucleus; these can then be coordinated to metal centers in either discrete complexes or extended arrays.[16]

It is well-established that the acetylenic diphosphine $Ph_2PC\equiv CPPh_2$ (dppa) is incapable of acting as a chelating ligand because of its linear nature, but when π-coordinated to a transition metal through the alkyne bond, the phosphine substituents are sufficiently bent back to act as a bidentate ligand to an additional metal.[17] We reasoned that by incorporation of this diphosphine into a dithiolene ligand using the methodology described above, the resulting rehybridization would afford potentially bidentate or tetradentate ligands. So it proved: reaction of dppa with **3a** afforded the complex $Mo_2\{\mu\text{-SC(CO}_2\text{Me)=C(CO}_2\text{Me)S}\}\{\mu\text{-SC(PPh}_2\text{)=C(PPh}_2\text{)S}\}Cp_2$ (**2g**) containing one diphosphine−dithiolene ligand, and similar treatment of **1** with an excess of the phosphine smoothly gave the bis(dithiolene) complex $Mo_2\{\mu\text{-SC(PPh}_2\text{)=C(PPh}_2\text{)S}\}_2Cp_2$ (**2h**) (Scheme 1). The presence of the diphosphine unit was clearly indicated by their ^{31}P NMR spectra, and also by the ^{13}C NMR spectrum of **2g** in which the dithiolene carbon atoms of the phosphine-substituted dithiolene ligand appear as doublets of doublets (ABX spin system). Reaction of **1** with 1 equiv of dppa gave the mixed dithiolene−dithiolate species $Mo_2\{\mu\text{-SC(PPh}_2\text{)=C(PPh}_2\text{)S}\}(\mu\text{-SCH}_2\text{CH}_2\text{S})Cp_2$ (**3c**), though the yield of this reaction was disappointingly low (19%); consequently, the chemistry of **3c** has not been investigated further.

Scheme 2. Synthesis of the Trinuclear Mo_2Ru Complex **4a**

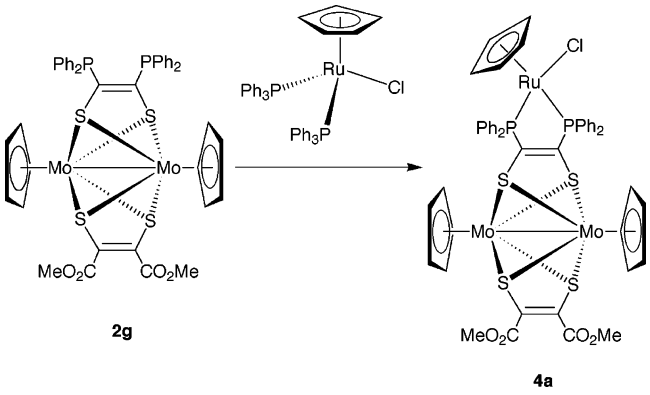

To explore the coordination of the new diphosphines, we selected a ruthenium(II) precursor, $CpRu(PPh_3)_2Cl$, based on the facts that (i) both PPh_3 ligands are easily displaced by diphosphines under relatively mild conditions to give good yields of complexes such as CpRu(dppe)Cl and (ii) the Ru(III)/Ru(II) redox couple is readily accessible for electrochemistry. Treatment of **2g** with 1 equiv of $CpRu(PPh_3)_2Cl$ in refluxing toluene for 5 h afforded a single orange product $Mo_2\{\mu\text{-SC(CO}_2\text{Me)=C(CO}_2\text{Me)S}\}\{\mu\text{-SC(PPh}_2\text{)=C(PPh}_2\text{)S}\}Cp_2(RuClCp)$ (**4a**) (Scheme 2) with a ^{31}P NMR peak at δ 60.8. Given that the corresponding peak in **2g** is at δ −10.1, this represents a coordination shift of 70.9 ppm, similar to the 82.3 ppm shift observed on coordinating free dppe (δ −12.2) to form CpRu(dppe)Cl (δ 70.1). Whereas in **2g** the two Cp ligands of the dimolybdenum core are equivalent, addition of the ruthenium fragment renders them inequivalent, hence the observation of three Cp signals in the ^1H and ^{13}C NMR spectra of **4a**.

In a similar manner, treatment of **2h** with 2 equiv of $CpRu(PPh_3)_2Cl$ afforded the tetrametallic complex $Mo_2\{\mu\text{-SC-}$

(14) McKenna, M.; Wright, L. L.; Miller, D. J.; Tanner, L.; Haltiwanger, R. C.; Rakowski Dubois, M. *J. Am. Chem. Soc.* **1983**, *105*, 5329.

(15) Reference 14 mentions an experiment of this type and contains a line drawing of one mixed bis(dithiolene) complex, $Mo_2(\mu\text{-SCH=CHS})(\mu\text{-SCH=CPhS})Cp_2$, but no experimental details or characterizing data were included.

(16) (a) Fourmigué, M.; Uzelmeier, C. E.; Boubekeur, K.; Bartley, S. L.; Dunbar, K. R. *J. Organomet. Chem.* **1997**, *529*, 343. (b) Smucker, B. D.; Dunbar, K. R. *J. Chem. Soc., Dalton Trans.* **2000**, 1309. (c) Fourmigué, M.; Batail, P. *Bull. Soc. Chim. Fr.* **1992**, *129*, 29.

(17) Powell, A. K.; Went, M. J. *J. Chem. Soc., Dalton Trans.* **1992**, 439.

Scheme 3. Synthesis of the Tetranuclear Mo_2Ru_2 Complex **4b**

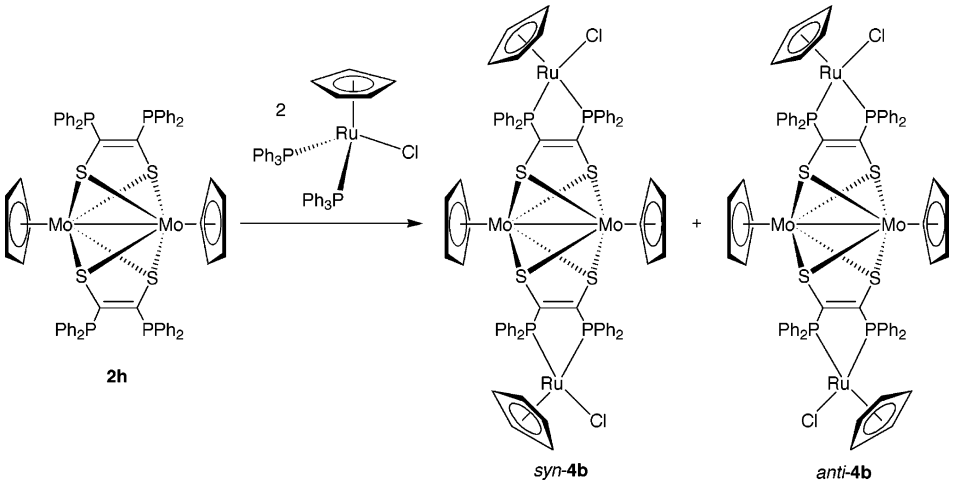

Scheme 4. Synthesis of the Pentanuclear Mo_4Ru Complex **5**

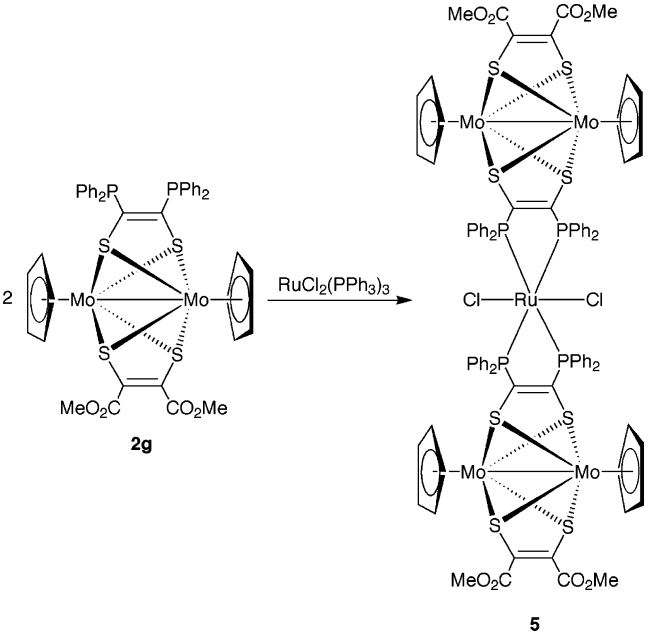

(PPh_2)═$C(PPh_2)S\}_2Cp_2(RuClCp)_2$ (**4b**) (Scheme 3). This compound can exist as two isomers depending on the relative orientation of the CpRuCl fragments (syn or anti). The two isomers were readily separated by column chromatography and are easily distinguished since in the syn isomer, the Cp ligands of the dimolybdenum core are inequivalent, whereas in the anti isomer they are equivalent. The Cp rings of the ruthenium moieties are equivalent in both isomers. The anti isomer was obtained in low yield (12%), but the yield of the more soluble syn isomer was considerably higher (38%). Both isomers gave appropriate mass spectra and elemental analysis data, and in addition, the X-ray structure of the syn isomer was determined (see below). No interconversion between the isomers was observed.

To investigate the possible construction of molecular wires from alternating Mo_2 and Ru units, the synthesis of pentametallic complex **5** was attempted (Scheme 4). On the basis of the fact that a convenient synthesis of *trans*-$RuCl_2(dppe)_2$ involves the addition of dppe to $[RuCl_2(PPh_3)_3]$ at room temperature in acetone, we envisaged that 2 equiv of the bidentate phosphine **2g** might react in a similar manner to give $RuCl_2\{Mo_2\{\mu$-$SC(CO_2Me)$═$C(CO_2Me)S\}\{\mu$-$SC(PPh_2)$═$C(PPh_2)S\}Cp_2\}_2$ (**5**). In the event, an orange-beige powder precipitated from the reaction mixture; acquisition of NMR data was impossible due to its insolubility, but a molecular ion peak was observed at *m*/*z* 2147 in its mass spectrum and a correct elemental analysis was obtained. It is therefore possible to envisage the formation of a polymeric molecular wire from $[RuCl_2(PPh_3)_3]$ and **2h** if the problem of insolubility could be overcome.

Crystallographic Studies. Two of the simple bis(dithiolene) complexes, centrosymmetric *trans*-**2c** and the mixed dithiolene species **2d**, were characterized crystallographically. The molecular structures are shown in Figures 1 and 2, respectively, with selected bond lengths and angles listed in the captions. Both complexes display geometries very similar to the previously studied $Mo_2\{\mu$-$SC(CF_3)$═$C(CF_3)S\}_2$-Cp_2 and $Mo_2(\mu$-SCH═$CHS)_2Cp_2$.[9,11] The two molybdenum atoms, both formally Mo(III), are linked by a bond of length 2.5832(6) Å in *trans*-**2c** (2.5848(8) Å in **2d**), which is typical for quadruply bridged complexes of this oxidation state.[18] This bond is bridged symmetrically by the four sulfur atoms, forming the familiar orthogonal arrangement of the two Mo_2S_2 planes with the dithiolene C═C bonds lying essentially perpendicular to the Mo−Mo axis. Each Mo atom thus lies in a four-legged piano stool environment. The C(6)−C(7) distance within the dithiolene ligands in *trans*-**2c** is 1.312(6) Å, experimentally indistinguishable from the corresponding bond lengths in **2d**.

Confirmation of the incorporation of dppa to form phosphine-substituted dithiolene ligands was provided by the crystal structures of both **2g** and **2h**, the results of which are detailed in Figures 3 and 4, respectively. The cores of the structures are very similar to those described above, with the dithiolene ligands perpendicular to the Mo−Mo bond. In each case, the phosphine substituents are clearly suitably aligned for coordination to additional metal centers. The

(18) Pétillon, F. Y.; Schollhammer, P.; Talarmin, J.; Muir, K. W. *Coord. Chem. Rev.* **1998**, *178*−*180*, 203.

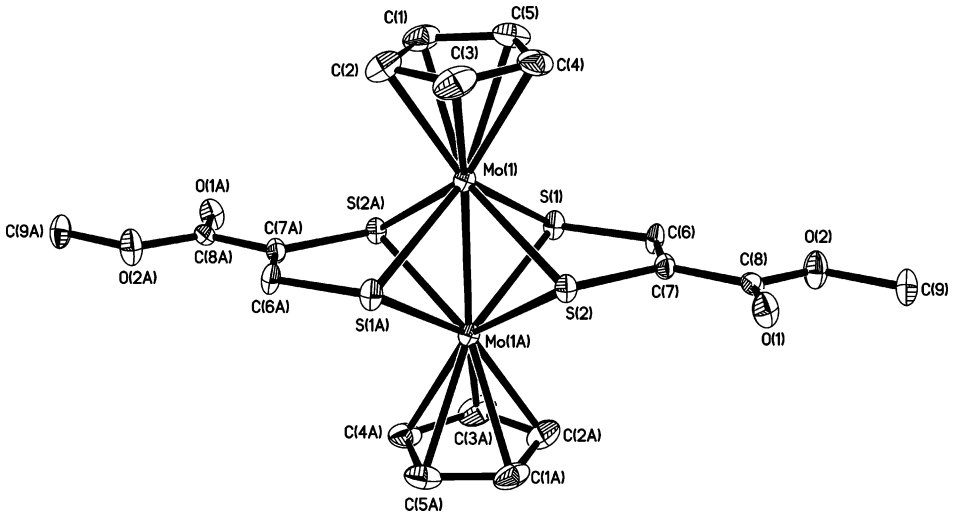

Figure 1. Molecular structure of the complex **2c** in the crystal (ORTEP plot, 50% probability ellipsoids). Hydrogen atoms have been omitted for clarity. Selected bond lengths and angles: Mo(1)−Mo(1A) 2.5832(6) Å, C(6)−C(7) 1.312(6) Å, av. Mo−S 2.464 Å, av. Mo−S−Mo 63.24°.

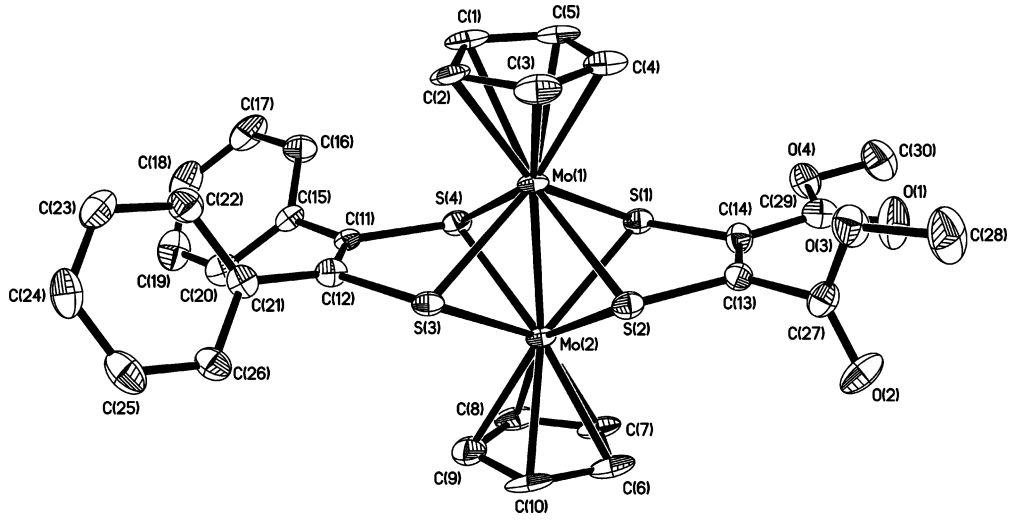

Figure 2. Molecular structure of **2d** in the crystal (ORTEP plot, 50% probability ellipsoids). Hydrogen atoms and a toluene solvent molecule have been omitted for clarity. Selected bond lengths and angles: Mo(1)−Mo(2) 2.5848(8) Å, Mo(1)−S(1) 2.464(2) Å, Mo(2)−S(1) 2.468(2) Å, Mo(1)−S(2) 2.472(2) Å, Mo(2)−S(2) 2.466(2) Å, Mo(1)−S(3) 2.444(2) Å, Mo(2)−S(3) 2.440(2) Å, Mo(1)−S(4) 2.457(2) Å, Mo(2)−S(4) 2.442(2) Å, C(11)−C(12) 1.338(9) Å, C(13)−C(14) 1.325(9) Å, Mo(1)−S(1)−Mo(2) 63.21(4)°, Mo(2)−S(2)−Mo(1) 63.13(4)°, Mo(2)−S(3)−Mo(1) 63.91(4)°, Mo(2)−S(4)−Mo(1) 63.69(4)°.

structures of **4a** and **4b** (Figures 5−7, Tables 1 and 2) show that coordination of the additional ruthenium fragments leaves the core of the molecules relatively unchanged. For example, in **4a**, the only significant changes are that the P(1)−C(16)−C(17) and C(16)−C(17)−P(2) angles in this ligand contract to an average of 117.3° from 123.5° in **2g**. A similar decrease in angles is observed on going from **2h** to **4b**. In **4a**, the S(1)−C(16) and S(2)−C(17) bonds of the phosphine dithiolene possibly shorten slightly to an average of 1.794 Å from 1.820 Å in **2g**, but this is at the limit of significance and is even less clear-cut in **4b**. The structure of **4b** seen from a viewpoint along the Mo−Mo bond (Figure 7) emphasizes the relative planarity of the core. The sulfur and phosphorus atoms, together with C(21)−C(24), are all effectively coplanar (mean deviation from this plane 0.1002 Å) with the ruthenium atoms displaced slightly to one side, Ru(1) by 0.7899 Å and Ru(2) by 0.8038 Å. The Ru−Ru separation is approximately 12.4 Å.

Electrochemical Studies. Cyclic voltammetry was carried out in dichloromethane solution on selected bis(dithiolene) complexes, with the results shown in Table 3. Complex **2a** exhibits a single reversible oxidation at 0.71 V vs AgCl/Ag, followed by irreversible oxidation processes at 1.36 and 1.63 V; it also displays an irreversible reduction at − 1.09 V. Previous electrochemical studies of the bis(dithiolene) complex $Mo_2(\mu\text{-SCH=CHS})_2Cp_2$ showed that it underwent a reversible oxidation at 0.23 V vs SCE;[9] in the C_5H_4Me analogue, this wave moved to 0.15 V and a second irreversible oxidation was observed at 0.64 V.[19] In the analogous $Mo_2\{\mu\text{-SC}(CF_3)\text{=C}(CF_3)\text{S}\}_2Cp_2$, the oxidation wave was at higher potential (0.88 V vs SCE) and an irreversible reduction (at −1.37 V) was also observed.[9] As expected, stepwise replacement of the electron-withdrawing CO_2Me substituents by PPh_2 groups is accompanied by a

(19) Casewit, C. J.; Haltiwanger, R. C.; Noordik, J.; Rakowski Dubois, M. *Organometallics* **1985**, *4*, 119.

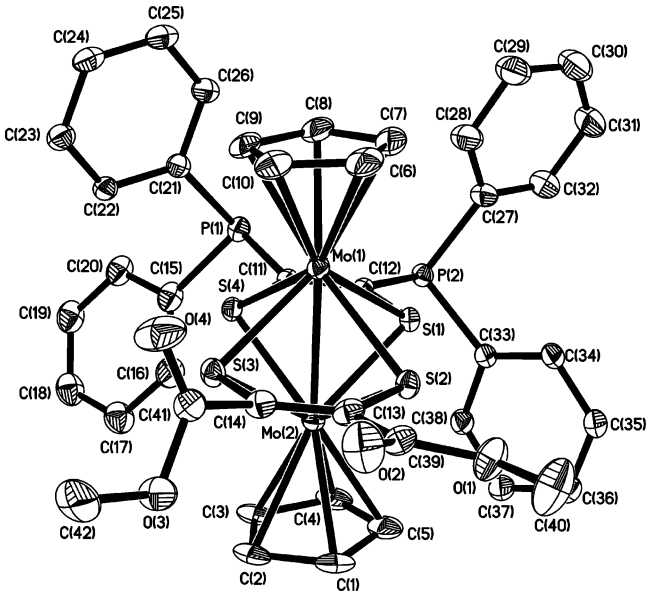

Figure 3. Molecular structure of **2g** in the crystal (ORTEP plot, 50% probability ellipsoids). Hydrogen atoms and a dichloromethane solvent molecule have been omitted for clarity. Selected bond lengths and angles: Mo(1)−Mo(2) 2.5901(9) Å, Mo(1)−S(1) 2.458(2) Å, Mo(2)−S(1) 2.438(2) Å, Mo(1)−S(2) 2.471(2) Å, Mo(2)−S(2) 2.443(2) Å, Mo(1)−S(3) 2.452(2) Å, Mo(2)−S(3) 2.461(2) Å, Mo(1)−S(4) 2.439(2) Å, Mo(2)−S(4) 2.456(2) Å, C(11)−C(12) 1.327(6) Å, C(13)−C(14) 1.295(8) Å, Mo(2)−S(1)−Mo(1) 63.87(4)°, Mo(2)−S(2)−Mo(1) 63.61(4)°, Mo(1)−S(3)−Mo(2) 63.63(4)°, Mo(1)−S(4)−Mo(2) 63.89(4)°, C(12)−C(11)−P(1) 123.1(5)°, C(11)−C(12)−P(2) 123.9(5)°.

progressive shift of the reversible oxidation to lower potential, viz., 0.71 V in **2a**, 0.59 V in **2g**, and 0.47 V in **2h**.

In **4a**, introduction of a ruthenium(II) fragment causes the appearance of a second reversible redox wave ($E_{1/2}$ 0.63 and 0.90 V). In complex **4b**, the two ruthenium centers are chemically equivalent, but the cyclic voltammogram displays three reversible oxidation processes at 0.57, 0.80 and 0.98 V vs AgCl/Ag (Figures 8 and 9); each of these oxidation processes is of the same area in the differential pulse voltammogram (i.e., they are all one-electron couples). The question then is which of these waves is associated with the dimolybdenum core and which is associated with the ruthenium centers.

In order to investigate the mixed-metal complexes in more detail, the spectroelectrochemistry of the redox couples was explored using the optically transparent thin-layer electrode (OTTLE) technique. Unfortunately, the low solubility of **2a** precluded the recording of a spectrum for this complex, but on oxidation of the more soluble η-C_5H_4Me analogue, peaks grew in at 12 700 cm^{-1} (790 nm) and 9760 cm^{-1} (1025 nm). Electrochemical oxidation of **4a** was carried out at 243 K at fixed voltages of 0.84 and 1.31 V; under these conditions, the redox changes were fully reversible. Parts a and b of Figure 10 show the spectroscopic changes observed for the first and second oxidations, respectively. The first is characterized by clear isosbestic points and the appearance of two low-energy charge-transfer bands at 12 200 and 9600 cm^{-1}, whereas the changes for the second oxidation are more subtle, with the first of these bands shifting to slightly higher energy (12 550 cm^{-1}).

Oxidation of **4b** was carried out at 253 K at potentials of 0.77, 0.96, and 1.39 V, under which conditions all changes were again fully reversible. The spectrum for the first oxidation is shown in Figure 11a and in common with that of **4a** shows the development of charge-transfer absorptions at 11 900 and 9300 cm^{-1} in a similar intensity ratio. Interestingly however, as shown in Figure 11b, the higher energy band largely disappears on oxidation to the dication and then reappears (at a higher energy of 12 550 cm^{-1}) on

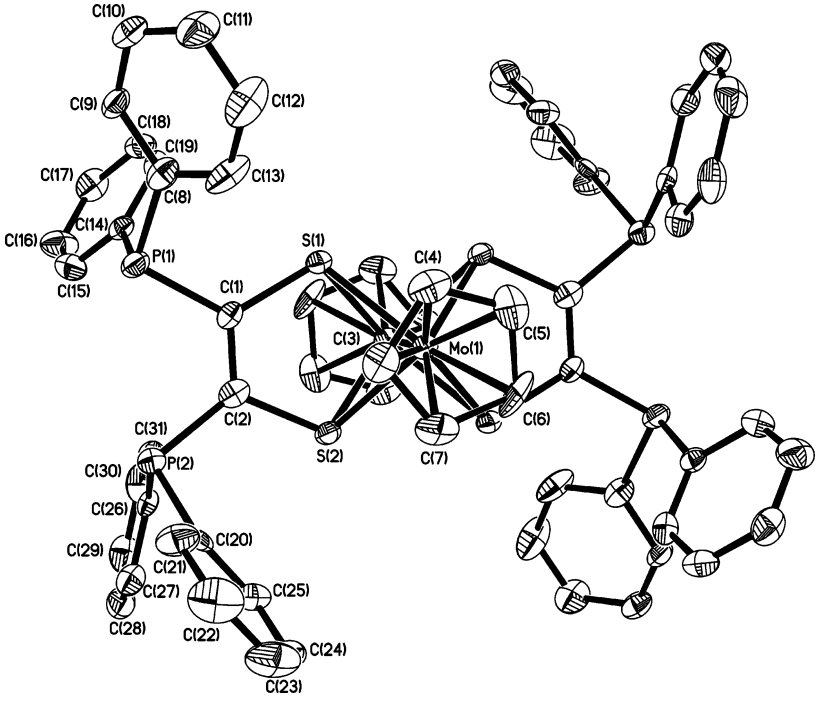

Figure 4. Molecular structure of **2h** in the crystal (ORTEP plot, 50% probability ellipsoids). Hydrogen atoms have been omitted for clarity. Selected bond lengths and angles: Mo(1)−Mo(1A) 2.586(1) Å, C(1)−C(2) 1.338(7) Å, av. Mo−S 2.447 Å, av. Mo−S−Mo 63.78°, C(1)−C(2)−P(2) 124.8(5)°, C(2)−C(1)−P(1) 121.2(4)°.

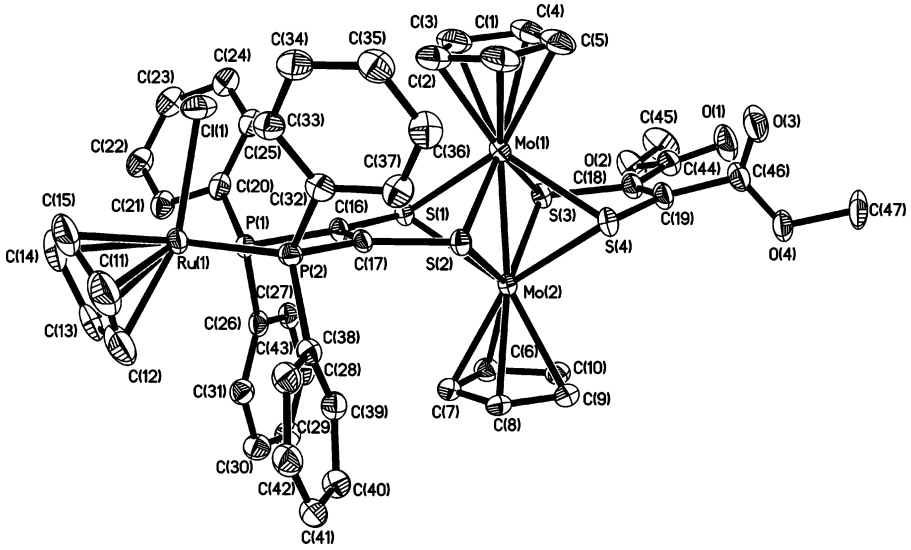

Figure 5. Molecular structure of the trinuclear complex **4a** in the crystal (ORTEP plot, 50% probability ellipsoids). Hydrogen atoms have been omitted for clarity.

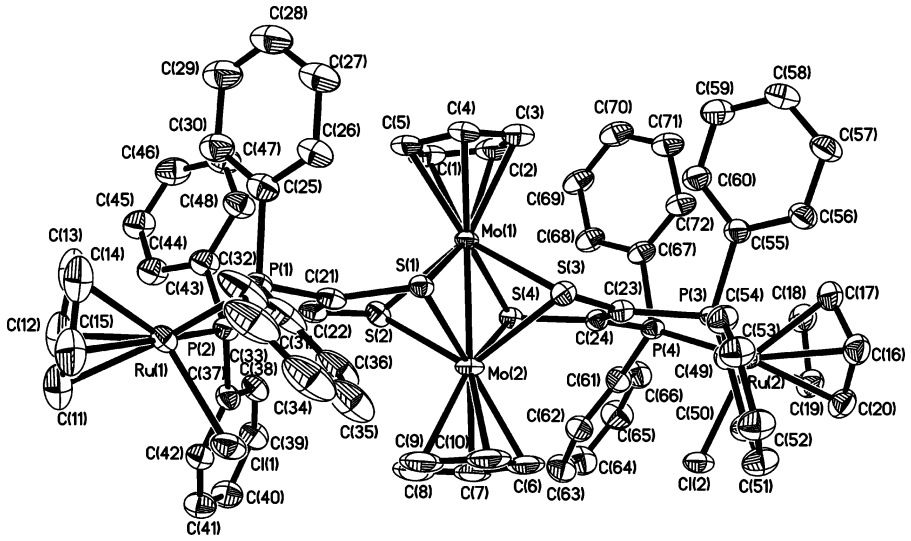

Figure 6. Molecular structure of the tetranuclear complex *syn*-**4b** in the crystal (ORTEP plot, 50% probability ellipsoids). Hydrogen atoms and the dichloromethane solvent molecules have been omitted for clarity.

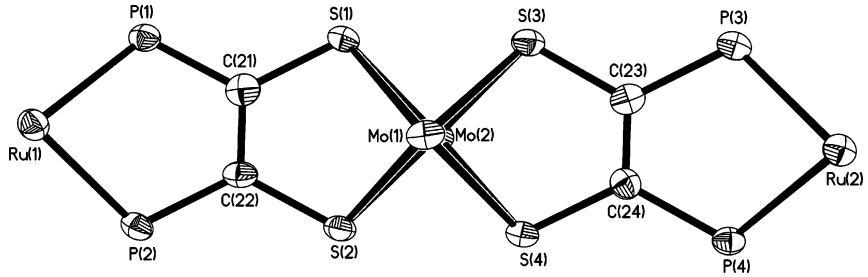

Figure 7. Structure of the core of *syn*-**4b**.

further oxidation to the trication, whereas the lower energy band remains relatively unchanged throughout. We defer discussion of these data until the DFT analysis has been introduced.

In a further attempt to examine the site of oxidation of **4a**, we recorded the X-band electron paramagnetic resonance (EPR) spectra of the radical cations of several of the complexes reported here. However, these experiments have so far been unhelpful, as the spectra have proved difficult to analyze. Some complexes (e.g., the C_5H_4Me analogue of **2a**, and **4a**) give a well-defined spectrum with g = approximately 2.01 with clearly observable Mo satellites (A_{Mo} approximately 28 G); however, superimposed on this is a second, much broader peak at around $g = 1.95$ with no discernible fine structure. The relative size of this second peak varies considerably from compound to compound, and in some cases (e.g., the cation of **4b**) it is the only one present. The size of the peak does not appear to depend on

Table 1. Selected Bond Lengths (Å) and Angles (deg) for the Trinuclear Complex **4a**

Mo(1)−S(2)	2.438(1)	Mo(1)−S(1)	2.463(1)
Mo(1)−S(4)	2.467(1)	Mo(1)−S(3)	2.470(1)
Mo(1)−Mo(2)	2.5990(8)	Mo(2)−S(2)	2.445(1)
Mo(2)−S(4)	2.458(1)	Mo(2)−S(3)	2.459(1)
Mo(2)−S(1)	2.470(1)	Ru(1)−P(2)	2.257(1)
Ru(1)−P(1)	2.263(1)	Ru(1)−Cl(1)	2.441(1)
C(16)−C(17)	1.339(5)	C(18)−C(19)	1.307(6)
P(2)−Ru(1)−P(1)	84.34(4)	P(2)−Ru(1)−Cl(1)	90.25(4)
P(1)−Ru(1)−Cl(1)	83.30(4)	Mo(1)−S(1)−Mo(2)	63.60(3)
Mo(1)−S(2)−Mo(2)	64.32(3)	Mo(2)−S(3)−Mo(1)	63.65(3)
Mo(2)−S(4)−Mo(1)	63.71(3)	C(17)−C(16)−P(1)	117.0(3)
C(16)−C(17)−P(2)	117.5(3)		

Table 2. Selected Bond Lengths (Å) and Angles (deg) for the Tetranuclear Complex *syn*-**4b**·$2CH_2Cl_2$

Mo(1)−S(1)	2.452(2)	Mo(1)−S(2)	2.468(2)
Mo(1)−S(4)	2.475(2)	Mo(1)−S(3)	2.480(2)
Mo(1)−Mo(2)	2.596(1)	Mo(2)−S(2)	2.451(2)
Mo(2)−S(3)	2.461(2)	Mo(2)−S(1)	2.464(2)
Mo(2)−S(4)	2.480(2)	Ru(1)−P(1)	2.260(2)
Ru(1)−P(2)	2.263(2)	Ru(1)−Cl(1)	2.434(2)
Ru(2)−P(4)	2.266(2)	Ru(2)−P(3)	2.271(2)
Ru(2)−Cl(2)	2.446(2)	C(21)−C(22)	1.349(8)
C(23)−C(24)	1.317(9)		
P(1)−Ru(1)−P(2)	83.76(6)	P(1)−Ru(1)−Cl(1)	83.94(6)
P(2)−Ru(1)−Cl(1)	89.20(6)	P(4)−Ru(2)−P(3)	83.59(6)
P(4)−Ru(2)−Cl(2)	85.37(6)	P(3)−Ru(2)−Cl(2)	91.34(6)
Mo(1)−S(1)−Mo(2)	63.76(4)	Mo(2)−S(2)−Mo(1)	63.72(5)
Mo(2)−S(3)−Mo(1)	63.40(5)	Mo(1)−S(4)−Mo(2)	63.21(4)
C(22)−C(21)−P(1)	115.9(5)	C(21)−C(22)−P(2)	118.2(5)
C(24)−C(23)−P(3)	118.1(5)	C(23)−C(24)−P(4)	117.3(5)

Table 3. Summary of Electrochemical Data for the New Complexes, V vs AgCl/Ag

complex[a]	reduction 1	oxidation 1	oxidation 2	oxidation 3
2a	$E_pc = -1.09$	$E_{1/2} = 0.71$	$E_pa = 1.36$	$E_pa = 1.63$
2g	$E_pc = -1.22$	$E_{1/2} = 0.59$	$E_pa = 1.34$	$E_pa = 1.50$
2h	$E_pc = -1.49$	$E_{1/2} = 0.47$	$E_pa = 1.27$	
4a	$E_pc = -1.18$	$E_{1/2} = 0.63$	$E_{1/2} = 0.90$	
4b		$E_{1/2} = 0.57$	$E_{1/2} = 0.80$	$E_{1/2} = 0.98$
$CpRu(PPh_3)_2Cl$		$E_{1/2} = 0.57$	$E_pa = 1.44$	

[a] Recorded under an N_2 atmosphere in CH_2Cl_2 solution with 0.3 M $[NBu_4][BF_4]$ as supporting electrolyte, at a scan rate of 100 mV s^{-1}. Ferrocene was used as an internal standard; the ferrocenium/ferrocene couple was measured at 0.55 V vs AgCl/Ag.

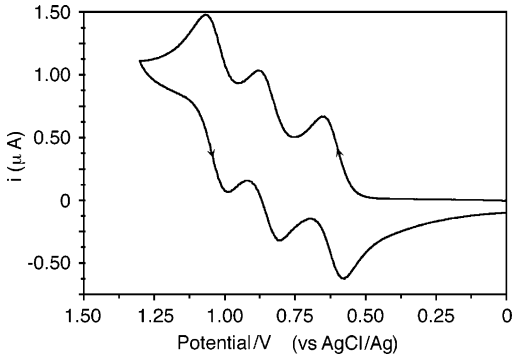

Figure 8. Cyclic voltammogram of complex **4b** in CH_2Cl_2 solution (0.3 M $[NBu_4][BF_4]$, scan rate of 100 mV s^{-1}, ferrocene as internal standard (not shown).

the size of the dithiolene substituents, the presence or absence of a ruthenium atom, or the method of cation generation (chemical or electrochemical).

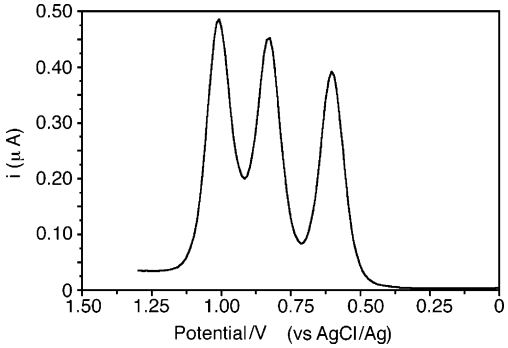

Figure 9. Differential pulse voltammogram of complex **4b**, same conditions as in Figure 8.

Electronic Structure and DFT Analysis (Parent Closed-Shell Species). The electronic structure of CpMo dimers with four bridging sulfur atoms has been previously studied, in relation to their UV−vis spectra, by Dubois and co-workers for complexes in which both metal atoms are Mo(III) or Mo(IV) and also for the mixed-valence Mo(III)−Mo(IV) state.[20−22] According to their molecular orbital picture, for a Mo(IV) dimer the highest-occupied molecular orbital (HOMO) is a b_{1u} orbital which is essentially composed of the δ^* interaction between the metal $d_{x^2-y^2}$ orbitals. Lying slightly above this, unusually, is the corresponding b_{2g} δ bonding interaction between the $d_{x^2-y^2}$ orbitals, which is destabilized by overlap with the p orbitals of the bridging sulfur atoms, and this forms the HOMO of the Mo(III) dimers. The UV−vis spectra of the Mo(III) dimers were relatively featureless, whereas the mixed-valence state was characterized by two reasonably intense absorptions in the regions of 7300−10000 and 13700−18400 cm^{-1} depending on the complex (though no bis(dithiolene) complexes were included in these earlier experiments). The lowest energy of these two bands was assigned to the δ^* to δ transition, which also contains some metal-to-ligand charge-transfer (MLCT) character. The previous discussion of the molecular orbital scheme for these quadruply bridged dimolybdenum species[20−22] used the same axis system shown in Figure 12 except that we define the *x* axis as bisecting the MoS_2 dithiolene rings. We work with two-fold symmetry that makes the two Mo atoms equivalent in species **2a**, whereas Dubois assumed four-fold symmetry. The two formally Mo(III) species each have three electrons to contribute to three molecular orbitals, which contained the paired six electrons. Our DFT calculations use the B3LYP functional and LanL2DZ basis set shown earlier by Cotton and co-workers[23,24] to be useful for dimolybdenum species. Moreover, in a detailed DFT study of molybdenum dithiolene species, both Hoffmann[25] and Wakamatsu[26] showed that

(20) Dubois, D. L.; Miller, W. K.; Rakowski Dubois, M. *J. Am. Chem. Soc.* **1981**, *103*, 3429.
(21) Casewit, C. J.; Rakowski Dubois, M. *Inorg. Chem.* **1986**, *25*, 74.
(22) Casewit, C. J.; Rakowski Dubois, M.; Grieves, R. A.; Mason, J. *Inorg. Chem.* **1987**, *26*, 1889.
(23) Cotton, F. A.; Murillo, C. A.; Villagrán, D.; Yu, R. *J. Am. Chem. Soc.* **2006**, *128*, 3281.
(24) Cotton, F. A.; Donahue, J. P.; Huang, P.; Murillo, C. A.; Villagrán, D. *Z. Anorg. Allg. Chem.* **2005**, *631*, 2606.
(25) Hofmann, M. *J. Mol. Struct. THEOCHEM* **2006**, *773*, 59.
(26) Wakamatsu, K.; Nishimoto, K.; Shibahara, T. *Inorg. Chim. Acta* **1999**, *295*, 180.

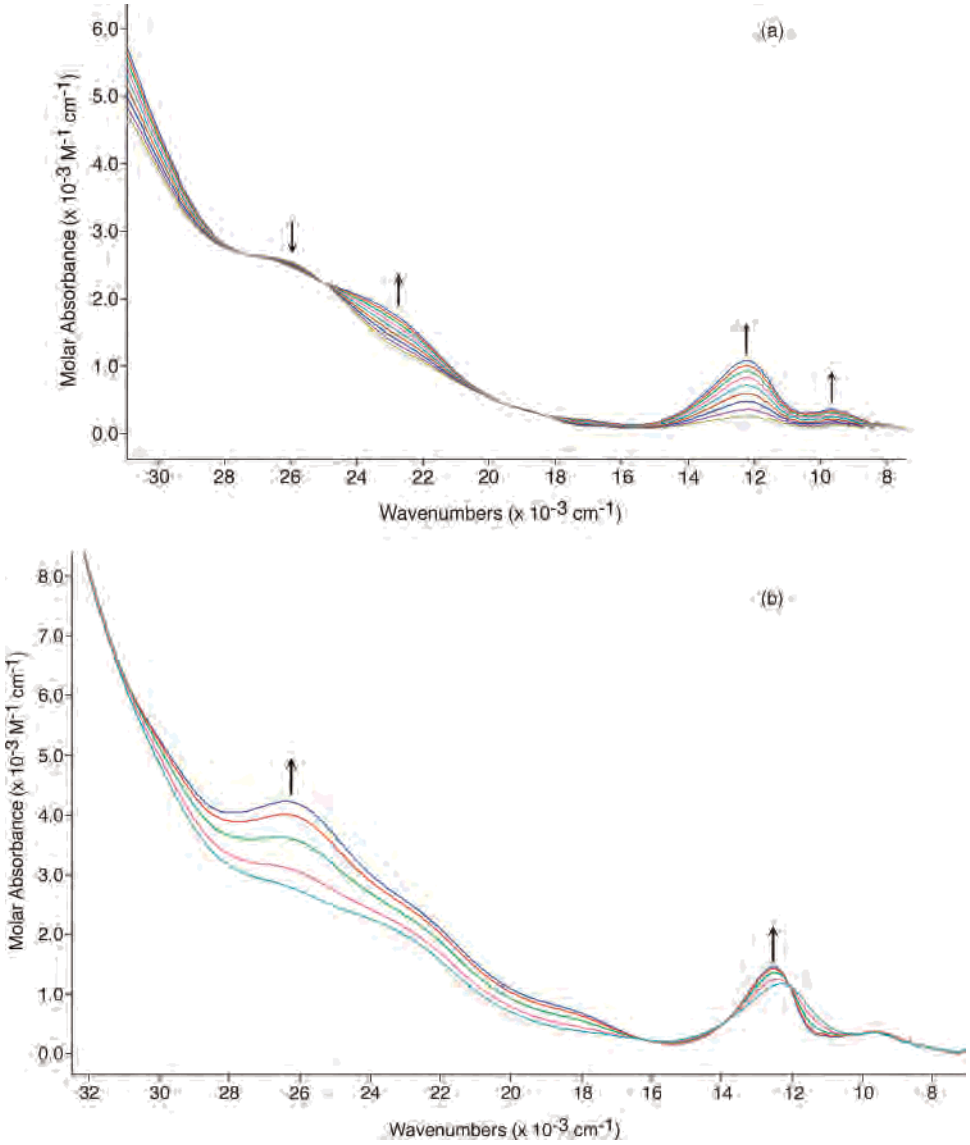

Figure 10. OTTLE spectra of complex **4a** recorded at 243 K in CH_2Cl_2 solution. (a) First oxidation (electrogeneration at 0.84 V). (b) Second oxidation (electrogeneration at 1.31 V).

B3LYP was one of the more useful functionals to use for molybdenum. Note also the successful use of B3LYP by Bitzer[27] for molybdenum systems.

Before discussing each species in turn, we note some general features illustrated in Figure 13a−d and listed in detail in the Supporting Information (Table S1). The three filled, predominantly molybdenum-localized orbitals can clearly be seen in each species. In all four species the dominant Mo−Mo bonding interaction is through overlap of the $<z^2>$ orbitals on each Mo, and there is δ overlap via the $<x^2-y^2>$ orbitals which leads to little if any net stabilization. The lowest-unoccupied molecular orbital (LUMO) is approximately 30% molybdenum in all the closed-shell species under discussion and comprises an antibonding $<xy> - <xy>$ composition. In the monoruthenium species **4a** there are, in addition, three filled mostly ruthenium-localized orbitals and in the diruthenium species *syn*-**4b**, six filled mostly ruthenium-localized orbitals. In both ruthenium species (**4a**, *syn*-**4b**), these orbitals occur at comparable energies (Table S1, Supporting Information) to the molybdenum-localized orbitals. There are only relatively small contributions from the cyclopentadienyl ligands to the filled frontier orbitals and little Cp contribution to the first few virtual unoccupied orbitals. The dominant ligand orbitals to these frontier levels derive mainly from the dithiolene ligand. The LUMO in all these species contains mostly ($<xy> - <xy>$), which also agrees with the Dubois analysis. Interestingly, these researchers used extended Hückel theory, which evidently performed well for these systems.

Species **2c**, Figure 13a (also see Table S1, Supporting Information) shows the three mainly molybdenum-localized orbitals as the HOMO (no. 105), HOMO-1, and HOMO-3 orbitals. By combination of the two symmetry-equivalent CpMo fragments, the dominantly metal-localized frontier filled orbitals comprising the metal−metal bond can be

(27) Bitzer, R. S.; Pereira, R. P.; Rocco, A. M.; Lopes, J. G. S.; Santos, P. S.; Nascimento, M. A. C.; Filgueiras, C. A. L. *J. Organomet. Chem.* **2006**, *691*, 2005.

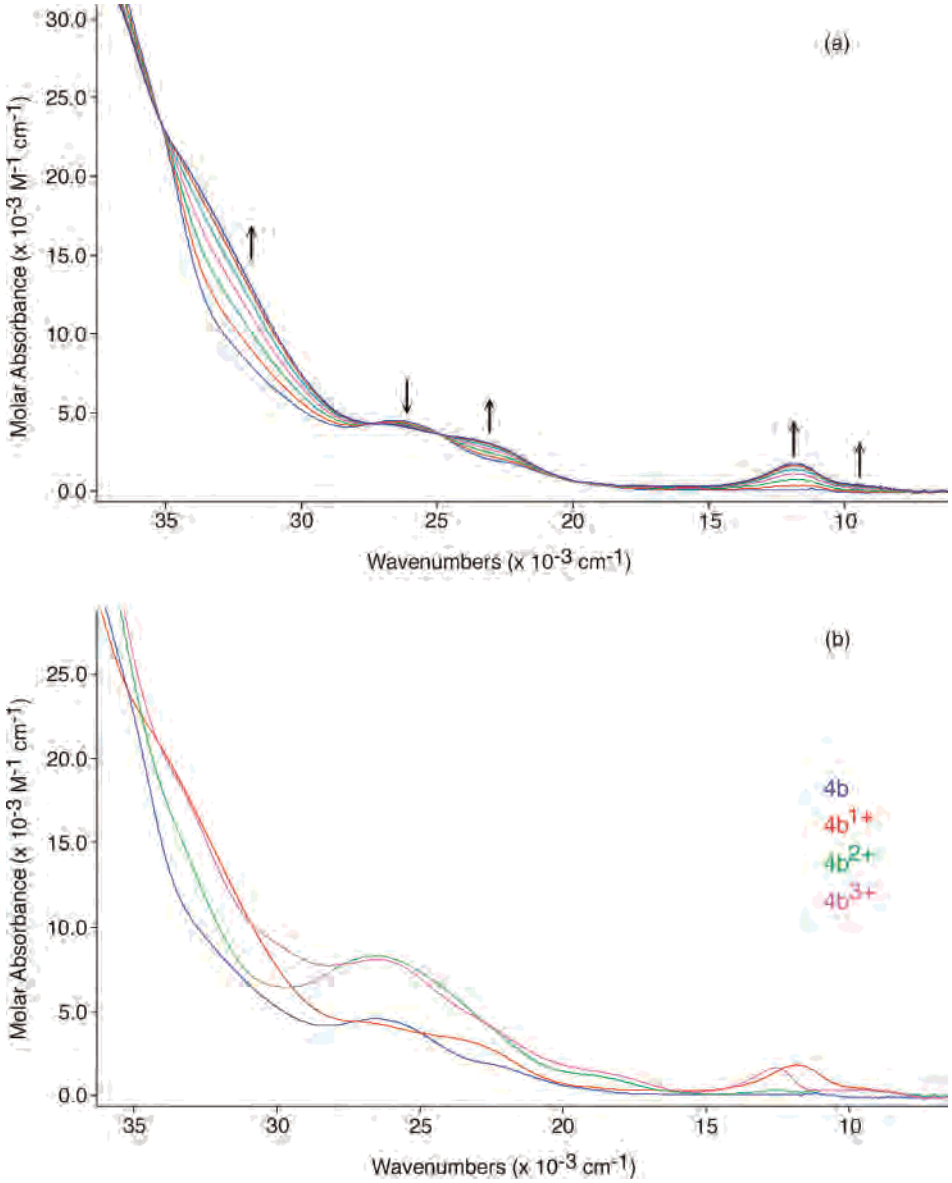

Figure 11. OTTLE spectra of complex **4b** recorded at 253 K in CH_2Cl_2 solution. (a) First oxidation (electrogeneration at 0.77 V). (b) Spectra of the three reversible oxidation products.

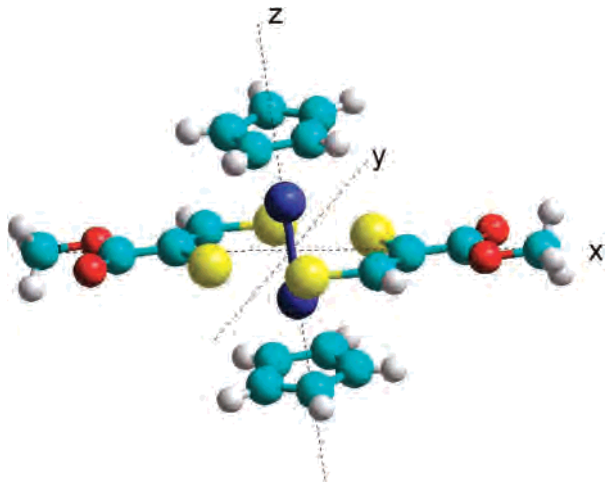

Figure 12. Axis coordinate system for species **2c**.

described as ($<z^2> + <z^2>$) (HOMO-3, σ-bonding) and then a pair of bonding (δ) and antibonding (δ^*) ($<x^2-y^2> + <x^2-y^2>$) (HOMO-1) and ($<x^2-y^2> - <x^2-y^2>$) (HOMO), respectively, providing a net bond order of 1. Although there is more than 30% Mo contribution to the LUMO, localized mostly on the dithiolene ligand, there is no net back-donation because the Mo $<xy>$ orbital is empty. While orbitals 105 (HOMO), 104, and 102 contain most of the molybdenum electron density (Figure 13a), molybdenum also contributes in a major way to many of the deeper lying orbitals (especially nos. 87, 88, 89, 91, 96, 97, 98). In species **2c**, these contain contributions from both Mo−Mo bonding and antibonding interactions.

In the tetraphosphine derivative **2h**, the three highest percentage molybdenum-localized orbitals (Figure 13b) are identified as the HOMO (no. 247) and HOMO-1, which are again the δ and δ^* coupled orbitals while the σ-bonding orbital is rather deeper at HOMO-5. Also, in this system, there are ligand-localized orbitals with substantial bonding and antibonding Mo_2 combinations.

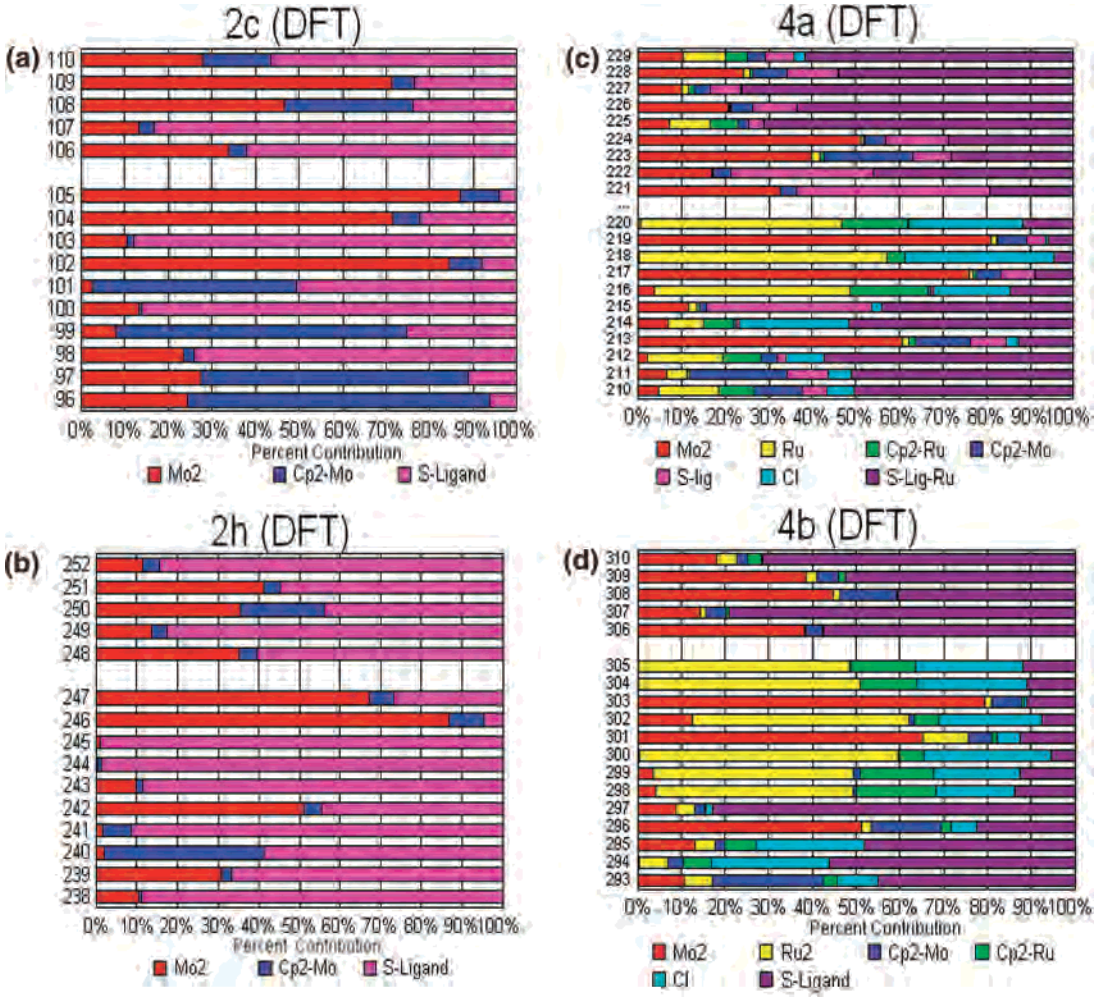

Figure 13. (a) Percent contribution in frontier molecular orbitals of species **2c** (DFT calculation). The left-hand index shows molecular orbital numbering with no. 105 as the HOMO and no. 106 as the LUMO. Contributions from molybdenum, sulfur ligand, and cyclopentadienyl ligands are color coded as shown. (b) Percent contribution in frontier molecular orbitals of species **2h** (DFT calculation). The left-hand index shows molecular orbital numbering with no. 247 as the HOMO and no. 248 as the LUMO. Contributions from molybdenum, sulfur ligand, and cyclopentadienyl ligands are color coded as shown. (c) Percent contribution in frontier molecular orbitals of species **4a** (DFT calculation). The left-hand index shows molecular orbital numbering with no. 220 as the HOMO and no. 221 as the LUMO. Contributions from molybdenum, ruthenium, sulfur ligand, with and without appended ruthenium atom, cyclopentadienyl ligands, attached to molybdenum or to ruthenium, and chloride are color coded as shown. (d) Percent contribution in frontier molecular orbitals of species **4b** (DFT calculation). The left-hand index shows molecular orbital numbering with no. 305 as the HOMO and no. 306 as the LUMO. Contributions from molybdenum, sulfur ligands with appended ruthenium atom, cyclopentadienyl ligands, attached to molybdenum or to ruthenium, and chloride are color coded as shown.

In the monoruthenium species **4a**, the HOMO (no. 220) is now primarily localized on ruthenium with the δ, δ^* orbitals (of somewhat distorted appearance due to the lack of symmetry of this species) being HOMO-1 and HOMO-3 and again offering no net bonding. The bonding $<z^2> + <z^2>$ orbital is HOMO-7 (no. 213) with two ruthenium-localized orbitals lying between it and HOMO-3 (Figure 13c). Thus, the three Ru-localized levels hold the d^6 configuration. The ruthenium-localized HOMO lies about 0.5 eV above the molybdenum-localized HOMO-1. Cyclopentadienyl orbitals from either the ruthenium- or molybdenum-bound cyclopentadienyl units contribute little to the frontier orbitals.

The diruthenium species (*syn*-**4b**) has a similar pattern, but now six mainly ruthenium-localized frontier orbitals are seen. The HOMO (no. 305) and HOMO-1 are both mainly ruthenium-localized and lie about 0.4 eV above HOMO-2, which is mainly molybdenum-localized (Figure 13d). In this case, the strongly σ-bonding Mo−Mo orbital is HOMO-9 (no. 296). In both **4a** and **4b**, there are no low-lying empty ruthenium-localized orbitals, but there are many which contain significant contributions from molybdenum.

Optical Spectra of Closed-Shell Species. Time-dependent DFT (TD-DFT) was used[26,28] to predict the electronic spectra of these species. We discuss the spectra of several of these species as representative of them all and deal here first with the uncharged closed-shell species. All exhibit a rather large number of weak overlapping charge transfer, relatively low energy, bands which generate the broad and weak unresolved visible region absorption seen with all these species. Detailed assignments can be found in Supporting Information (Table S2). Species **2c** is representative of the simplest species in this group. The TD-DFT-predicted visible region spectrum and experimental spectrum are shown in Figure 14a where the vertical bars show the locations of the electronic

(28) Vlcek, A., Jr.; Zális, S. *Coord. Chem. Rev.* **2007**, *251*, 258.

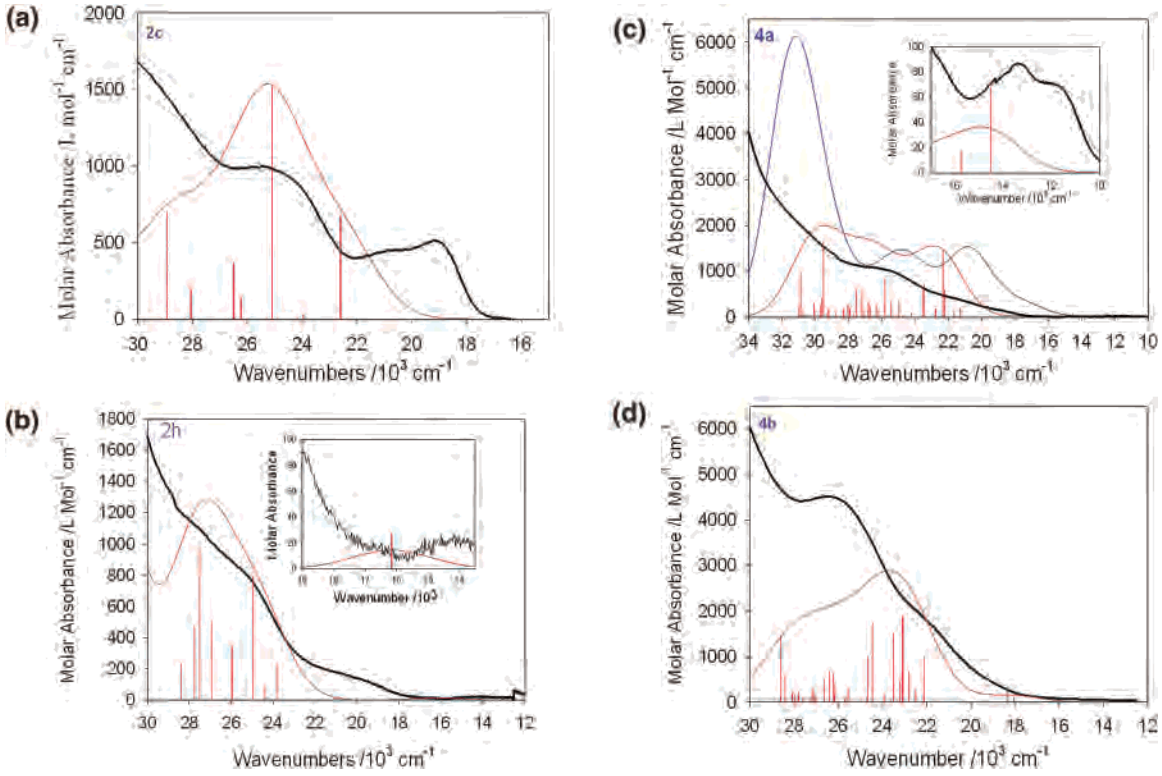

Figure 14. (a) Experimental spectrum of species **2c** in dichloromethane (black line) and TD-DFT calculated spectrum (red line) based upon the X-ray structure. The vertical bars are the locations of individual transitions scaled to the absorbance axis. In Figures 14a−d and 15a,b the upper limit of the TD-DFT calculated spectrum is determined by the number of excited states derived. The falloff at high wavenumber is not real but reflects the termination of the calculation. (b) Experimental spectrum of species **2h** in dichloromethane (black line) and TD-DFT calculated spectrum (red line) based upon the X-ray structure. The vertical bars are the locations of individual transitions scaled to the absorbance axis. Inset shows expansion of the short wavelength end of the spectrum. (c) Experimental spectrum of species **4a** in dichloromethane (black line), TD-DFT calculated spectrum (red line) based upon the X-ray structure, and TD-DFT calculated spectrum (blue line) based upon the B3LYP-geometry-optimized structure. The vertical bars are the locations of individual transitions scaled to the absorbance axis. Inset shows expansion of the short wavelength end of the spectrum. (d) Experimental spectrum of species **4b** in dichloromethane (black line) and TD-DFT calculated spectrum (red line) based upon the X-ray structure. The vertical bars are the locations of individual transitions scaled to the absorbance axis.

transitions. Even in this simple species, there are many low energy but weak predicted transitions. The three more intense bands at 22 600, 25 100, and 28 900 cm^{-1} can be assigned, predominantly, as MLCT Mo → S-ligand, $\pi-\pi^*$ (S-ligand) (with some LMCT character), and mixed MLCT, d−d, recognizing that fairly extensive mixing is occurring between metal and ligand orbitals. The pattern of the first three predicted transitions with two moderately intense bands and a weak band (at ca. 24 000 cm^{-1}) between them is mimicked by the experimental spectrum with two obvious peaks and a weak shoulder between them. These three experimental features are then reasonably associated with the first three predicted transitions.

Figure 14b compares the visible region experimental and TD-DFT predicted spectrum of the tetraphosphine **2h**. The two broad weak shoulders tailing into the visible region are quite well reproduced by the DFT predicted spectrum but again there are many predicted weak transitions in this region. The two most intense ones at 25 000 and 27 500 cm^{-1} are both primarily $\pi-\pi^*$ (S-ligand) with some LMCT character, the latter due to the presence of significant metal 4d character in the LUMO and LUMO+1. The very weak band shown in the inset to Figure 14b is the HOMO to LUMO transition (no. 247 → no. 248 in Figure 13b) which is a molybdenum d−d transition mixed with MLCT Mo → S-ligand.

Figure 14c shows the comparison of the visible region experimental and TD-DFT predicted spectrum of the mono-ruthenium diphosphine **4a**. This is an asymmetric molecule with a "bare" dithiolene ligand that does not have an appended ruthenium and one that does (Table S2, Supporting Information). The LUMO is primarily localized on the bare dithiolene ligand without appended ruthenium. Again, there are a plethora of fairly weak transitions below 30 000 cm^{-1} generating the broad-structured experimentally observed band. Although the HOMO is ruthenium-localized, the lowest two transitions (predicted 14500(0.0004) and 15700(0.0001) cm^{-1} (oscillator strength in parenthesis)) are MLCT from molybdenum-localized orbitals to the LUMO (Mo → π^* dithiolene) mostly on the bare dithiolene ligand but also with molybdenum d−d character (see Figures 13c and 14c inset). The next transition (17200(0.0002) cm^{-1}) is mostly Ru → π^* dithiolene, followed by one at 21300(0.0012) cm^{-1}, which is significantly more intense and is predominantly Ru → π^* dithiolene (bare). The Mo → π^* transitions lie at lower energy than excitations from ruthenium because of the considerable Coulombic penalty in moving charge from ruthenium to π^* dithiolene on the other side of the molecule. As the figure shows, there follow many transitions which are (Table S2, Supporting Information) mostly MLCT in character; there is a predicted $\pi-\pi^*$ (bare) dithiolene

transition at 25800(0.0049) cm^{-1}. The fairly intense transition at 22300(0.0086) cm^{-1} is a rather mixed transition but with a major MLCT Ru → π* dithiolene (with appended Ru) component. There is overall good agreement between the experimental and predicted spectra, especially in regard to the two, weak, low-energy transitions shown in Figure 14c (inset).

Figure 14d compares the visible region experimental and TD-DFT-predicted spectrum of the more symmetric di-ruthenium tetraphosphine complex *syn*-**4b**. Both HOMO and HOMO-1 are ruthenium-localized, but the first two predicted, but weak, transitions (15100(0.0001) and 15800(0.000) cm^{-1}) are MLCT (but with molybdenum d−d character) from HOMO-2 and HOMO-4, both of which are molybdenum-localized, to the LUMO, which mostly lies on the dithiolene ligand. The third predicted transition, substantially higher in energy (18000(0.0005) cm^{-1}), is the first ruthenium-to-dithiolene MLCT transition. There follow many transitions, almost all of which, up to 30 000 cm^{-1}, are MLCT from either Ru or Mo. The most intense in this grouping (23100-(0.0095) cm^{-1}) (HOMO → LUMO+1) is predominantly Ru → dithiolene MLCT.

DFT Analysis (Open-Shell Oxidized Species). Oxidation of species **2a**: As a control model, a spin-unrestricted DFT geometry optimization was carried out for the first oxidation product of species **2a**, again using the B3LYP functional and LanL2DZ basis set. The optimized species, **2a**$^+$, has C_2 symmetry, and the derived net spin density is distributed primarily and equally over both molybdenum atoms (0.60 e each). There is some negative spin density on the S ligating atoms.

Oxidation of species **4a**: There is uncertainty whether oxidation of this species is localized on the dimolybdenum center or on the ruthenium moiety. We therefore carried out an unrestricted-spin DFT geometry optimization of the oxidized species (**4a**$^+$) and also carried out a restricted-spin DFT geometry optimization of the ruthenium(II) precursor, species **4a**, for comparative purposes, to provide some confidence that the **4a**$^+$ calculation was valid. It is also useful in this context to compare the expected electronic spectrum of the DFT-optimized species **4a** with the spectrum predicted for the X-ray geometry. It is considered preferable to use a good DFT-optimized structure rather than the X-ray structure for the prediction of solution electronic spectra since the geometry in the solid may be constrained by packing phenomena. We observe (Figure 14c) similar electronic spectroscopic predictions for the two geometries but with the overall band envelope displaced somewhat to lower energy using the DFT-optimized geometry. The Mo−Mo distance in the optimized geometry of **4a** is 262 pm while the average Mo−S bond distance is 257 pm, the Ru−P distance is 240 pm, and the Ru−Cl distance is 253 pm. These can be compared with distances of 260, 246, 226, and 244 pm, respectively, in the X-ray structure.

In the DFT-optimized oxidation product **4a**$^+$, these distances are 263, 256−260, 244−245, and 241 pm, respectively. The singly occupied molecular orbital (SOMO) is localized at the ruthenium center. In agreement with this, the spin density at the ruthenium atom is 0.76 e, while there is no significant spin density at the molybdenum or sulfur atoms. A small positive spin density is found on chloride. Thus, the first oxidation process occurs at ruthenium in the gas-phase-optimized structure. Oxidation at ruthenium causes no large change in the Ru−P distance probably because of the rigidity of the ligand, but the Ru−Cl bond shortens considerably (relative to DFT-optimized **4a**).

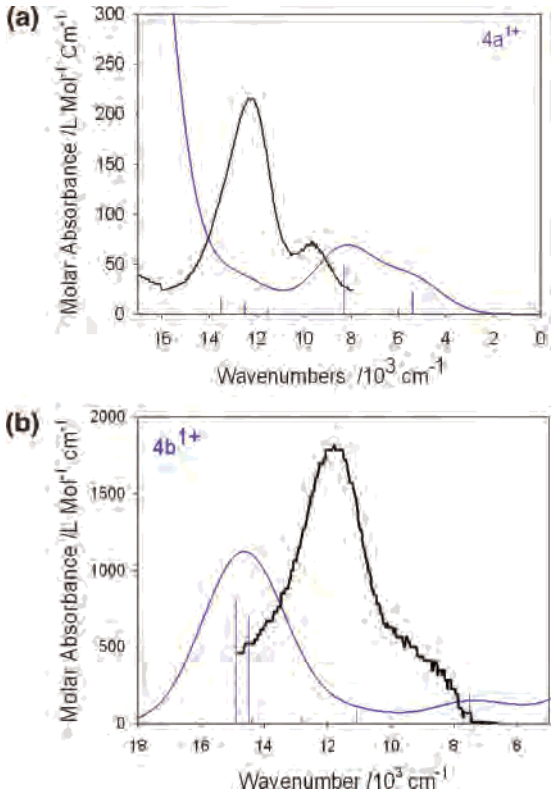

Figure 15. (a) Experimental spectrum of species **4a**$^+$ in dichloromethane (black line) and TD-DFT-calculated spectrum (blue line) based upon the B3LYP-geometry-optimized structure. The vertical bars are the locations of individual transitions scaled to the absorbance axis. (b) Experimental spectrum of species **4b**$^+$ in dichloromethane (black line) and TD-DFT-calculated spectrum (blue line) based upon the B3LYP-geometry-optimized structure. The vertical bars are the locations of individual transitions scaled to the absorbance axis.

The predicted optical spectrum of **4a**$^+$ is compared with the experimental spectrum in Figure 15a. Although shifted to lower energy relative to the experimental data, the overall band envelopes at lower energy, below 20 000 cm^{-1} (exp.), are closely similar, with two peaks and a higher energy shoulder. The lowest-energy band is mostly excitation no. 214B → no. 220B (B = β spin), which is a composite d−d and Cl → d LMCT transition. The next and stronger band is highly mixed and cannot be simply designated. The dominant component of this stronger transition (28% of the excitation) is mostly a phosphine-ligand-to-Ru LMCT transition. The trio of bands that create the higher energy shoulder are S-ligand (no pendant Ru)-to-Ru LMCT, a mixed transition not easily described, and Mo → Ru M′MCT.

Oxidation of species **4b**: In the DFT-optimized oxidation product **4b**$^+$, the spin density is again localized on ruthenium, equally between the two at 0.37 e each, with 0.09 e on each chloride and no significant spin density on molybdenum,

phosphorus or sulfur, or elsewhere. The SOMO is localized equally at the two ruthenium centers. The key distances are 263 pm (Mo−Mo), 257−260 pm (Mo−S), 242 pm (Ru−P), and 246 pm (Ru−Cl). Comparison of the calculated and experimental electronic spectrum in the low-energy region (6000−16000 cm^{-1}) is shown in Figure 15b. Good agreement is seen between the overall band envelope and energy, though the predicted intensities in this region are much lower than those actually observed. The weak lowest-energy component is a d−d transition (no. 297B → no. 305B) (with some ligand $\pi-\pi^*$ character) within what, in a mononuclear Ru(III) species, would be the t_{2g}^5 manifold as is typical for Ru(III) species.[29] The stronger band comprises two components, no. 304B → no. 306B, and no. 295B → no. 305B. The former is a mix of Ru → ligand MLCT and intermetallic Ru → Mo transition. The latter is mostly ligand-to-Ru(III) LMCT. There are very weak lower-lying Mo → ligand MLCT transitions predicted in the near-infrared region.

The highest-energy-available electron in $\mathbf{4b}^+$ is a β electron on ruthenium, suggesting that the next oxidation process to make $\mathbf{4b}^{2+}$ is oxidation of the second ruthenium center. For further characterization, the species $\mathbf{4b}^{2+}$ (assumed $S = 0$) and $\mathbf{4b}^{3+}$ (assumed $S = {}^1/_2$) were geometry-optimized and briefly analyzed. The LUMO on $\mathbf{4b}^{2+}$ is on ruthenium in agreement with the supposition that it is a Ru(III)···Ru(III) species. In $\mathbf{4b}^{3+}$, the spin density is primarily on both ruthenium centers and on one molybdenum center, suggestive then of a Ru(III)···Ru(III)···Mo(III)−Mo(IV) species.

Electrochemical assignments: It is now straightforward to assign the observed electrochemical data (Table 3). The first two oxidation processes observed with species **2a**, **2g**, and **2h** must be molybdenum-localized to form Mo(III)−Mo(IV) mixed-valence and Mo(IV)−Mo(IV) species; ligand oxidation does not occur at such a low positive potential. The third oxidation process seen with species **2a** and **2g** may be molybdenum-based, but it could also be ligand-based and we have no information to decide which is correct.

The first oxidation process in species **4a** and **4b** could obviously be either molybdenum- or ruthenium-localized. The ruthenium oxidation in $CpRu(PPh_3)_2Cl$ occurs at 0.57 V (Table 3), a value comparable to the first oxidation process in species **4a** and **4b**. The DFT analysis above clearly shows that the HOMO in both **4a** and **4b** is ruthenium-localized. Moreover, DFT calculations of the open-shell $\mathbf{4a}^+$ and $\mathbf{4b}^+$ both show unpaired spin density localized on ruthenium and not on molybdenum. In the case of $\mathbf{4b}^+$, the spin density is evenly shared between the two ruthenium atoms but this is a characteristic of the high symmetry; the two ruthenium atoms are essentially equivalent, and this does not, in itself, necessarily indicate delocalization across the molecule. It is possible that the solution species **4a** and **4b** differ from the gas-phase DFT calculation and that the frontier orbitals therein are molybdenum- and not ruthenium-localized, but this is unlikely since there is no especial reason for this to be the case. Moreover, the predicted electronic spectra of species $\mathbf{4a}^+$ and $\mathbf{4b}^+$ in the characteristic long-wavelength region (Figure 15) agree well in band shape and reasonably well in energy with the ruthenium-localized predicted spectra. Thus, the first oxidation processes (Table 3) in both **4a** and **4b** are assigned as Ru(II) oxidation to Ru(III).

The second oxidation process in $CpRu(PPh_3)_2Cl$ is more than 1 V more positive than the first while the second oxidation process in **4a** is only 0.23 V more positive than the first; it is then evidently molybdenum-localized.

The second oxidation process of **4b** to produce $\mathbf{4b}^{2+}$ evidently also takes place on ruthenium, producing the Ru(III)···Ru(III) species as indicated by the DFT data above. Comparison with the data obtained for $CpRu(PPh_3)_2Cl$ shows that the third oxidation process is too close to the second to be ascribed to the formation of Ru(IV), and this information and the DFT data described above show that the third oxidation process must be molybdenum-localized, forming the Ru(III)···Ru(III)···Mo(III)−Mo(IV) species $\mathbf{4b}^{3+}$.

The above analysis reveals communication between the two ruthenium centers in **4b**. The presence of three one-electron oxidation processes for this species requires, unequivocally, coupling of the two ruthenium sites across the dinuclear molybdenum site unless one supposed that two of the processes were molybdenum-localized, and the calculations rule that out. Thus, despite their separation by the dinuclear molybdenum site, the two ruthenium atoms do communicate. Assuming that the first two oxidation processes in **4b** are ruthenium-localized, then using $E_2 - E_1 = (RT/nF)\ln K_c$, the comproportionation constant for the process

$$[\mathrm{Ru(II)\cdot Ru(II)}] + [\mathrm{Ru(III)\cdot Ru(III)}] = 2[\mathrm{Ru(II)\cdot Ru(III)}]$$

is $K_c = 7.7 \times 10^3$. This, not too surprisingly, is on the low end of a range of K_c values for a variety of bridging ligands linking ruthenium centers, summarized by Sarkar and Kaim.[30] It does, however, exceed other simple, even short, bridging ligands such as a triazole dicarboxylic acid ligand ($K_c = 1.1 \times 10^3$).[31] The K_c value is not insignificant given the separation of the two ruthenium centers, about 124 pm, linked via a complex network of phosphorus, carbon, sulfur, and molybdenum atoms. Crutchley reported[32] values of K_c in the range of 10−68400, as a function of solvent, for a dicyanamide mixed-valence $(NH_3)_5Ru(III)/Ru(II)$ species with a similar Ru(III)···Ru(III) intermetallic distance, but in this case, linked by an unsaturated pathway.

Conclusions

In this work, we have demonstrated the generality of the stepwise reaction of $Mo_2(SCH_2CH_2S)_2Cp_2$ with two different alkynes to give complexes with two different dithiolene ligands. In this way, virtually complete control over the substituents R^1-R^4 can be achieved. The use of the acetylenic phosphine dppa has allowed the incorporation of phosphine substituents into dithiolene ligands for the first time. In principle, it should be possible to extend this

(29) Lever, A. B. P. *Inorganic Electronic Spectroscopy*; Elsevier Science: Amsterdam, 1984.

(30) Kaim, W.; Sarkar, B. *Coord. Chem. Rev.* **2007**, *251*, 584.
(31) Baitalik, S.; Dutta, B.; Nag, K. *Polyhedron* **2004**, *23*, 913.
(32) Naklicki, M. L.; Crutchley, R. J. *J. Am. Chem. Soc.* **1994**, *116*, 6045.

synthetic route to other complexes where dithiolene ligands are constructed from sulfido ligands and alkynes, though two potential problems are first, the coordination of the dppa to the metal center through the phosphorus atoms and second, the oxidation of the phosphine units to $P(=S)Ph_2$ groups in reactions that contain elemental sulfur. It is also shown that the resulting complexes can be employed as bidentate or tetradentate ligands to other metal fragments and that by judicious choice of a redox-active fragment, a degree of communication between two metal centers through the dimolybdenum dithiolene framework can be observed.

Overall, the DFT analysis provides a greater in-depth look at the electronic structures of these species. The electronic spectra are shown to be extremely complicated, with many weak low-energy transitions occurring close together and hence responsible for the broad unresolved structure seen in the visible-region electronic spectra. However, there is good quantitative agreement between the observed visible-region spectra and the predicted DFT spectra. Oxidation of both species **4a** and **4b** apparently occurs at ruthenium, which is not a conclusion readily reached from a simple consideration of the electrochemical potentials.

Future papers will address the communication between different types of redox-active units across the same Mo_2 framework and also our attempts to discover a more general way to produce such dithiolene ligands so that they can be coordinated to a wider range of central linking units.

Experimental Section

Materials. General experimental techniques were as described in recent work from this laboratory.[6] All reactions were routinely carried out under an argon or nitrogen atmosphere, though separation procedures were carried out without any special precautions since the products described are all relatively air-stable. Column chromatography was carried out on silica columns (Merck Kieselgel 60 or equivalent) made up initially in light petroleum; elution was then carried out with increasing proportions of dichloromethane. Light petroleum refers to the fraction boiling in the range 60−80 °C. Solvents were purified by either distillation from appropriate drying agents or a Grubbs-type purification system manufactured by Innovative Technology, Newburyport, MA. The complexes $Mo_2(SCH_2CH_2S)_2Cp_2$, $CpRu(PPh_3)_2Cl$, and $RuCl_2(PPh_3)_3$ were prepared by literature methods.[33−35] Bis(diphenylphosphino)acetylene, $Ph_2PC{\equiv}CPPh_2$, was prepared by the reaction of $LiC{\equiv}CLi$ with PPh_2Cl.[36] All other chemicals were obtained from commercial sources and used as supplied.

Physical Measurements. The ^1H and ^{13}C NMR spectra were obtained in $CDCl_3$ solution on a Bruker AC250 Fourier transform machine with an automated sample-changer or on a Bruker AMX400 spectrometer. Chemical shifts are given on the δ scale relative to $SiMe_4 = 0.0$ ppm. The $^{13}C\{^1H\}$ NMR spectra were routinely recorded using an attached proton test technique (JMOD pulse sequence). Mass spectra were recorded on a Fisons/BG Prospec 3000 instrument operating in fast atom bombardment mode with *m*-nitrobenzyl alcohol as the matrix; the figures reported are the highest intensity peak of each isotope envelope. Electrospray mass spectra were obtained on an LCT instrument. UV−vis absorption spectra were recorded on a Varian Cary 50 instrument in the range of 200−800 nm in dichloromethane solution with a path length of 1 cm. The X-band EPR spectra were recorded at the University of Manchester on a Bruker EMX hybrid spectrometer and simulated with Bruker's *Xsophe* software. Elemental analyses were carried out by the Microanalytical Service of the Department of Chemistry at Sheffield with a Perkin-Elmer 2400 analyzer. Electrochemical experiments were carried out in N_2-purged dichloromethane (freshly distilled from CaH_2) with 0.3 M $[Bu_4N][BF_4]$ as supporting electrolyte. A standard three-electrode system was used with a Pt microdisc and a large surface area Pt wire as the working and counter electrodes, respectively. The reference electrode was AgCl/Ag in a solution of 0.45 M $[Bu_4N][BF_4]$ and 0.05 M $[Bu_4N][Cl]$, linked to the bulk solution by a fritted tube. At the end of every experiment, ferrocene was added as an internal standard. The ferrocenium/ferrocene couple was observed at 0.55 V vs AgCl/Ag.[37] Electrochemical reversibility was determined by scan rate dependency, with all potentials quoted for a scan rate of 100 mV s^{-1}. Processes are described as reversible if $\Delta E < 100$ mV and $|I_pa/I_pc| = 1$. The in situ UV−vis−near IR spectroelectrochemical experiments were carried out with an OTTLE cell using a Pt−Rh gauze as the working electrode, Pt wire as the counter electrode, and AgCl/Ag as the reference electrode in a temperature-controlled 0.5 mm quartz cell. At the end of the experiment, the applied voltage was returned to zero and the original spectrum was regenerated to ensure the reversibility of the processes.

Synthesis of $Mo_2\{\mu$-SC(CO$_2$Me)=C(CO$_2$Me)S$\}_2Cp_2$ (2a). A solution of complex **1** (360 mg, 0.712 mmol) and DMAD (0.3 mL) in CH_2Cl_2 (40 mL) was heated to reflux for 24 h. The solvent was removed in vacuo, and the residue was separated by column chromatography. A red band, eluted with acetone/CH_2Cl_2 (1:99), yielded 299 mg (57%) of **2a**. The characterizing data for this complex matched those given in the literature.[12]

Synthesis of $Mo_2(\mu$-SCPh=CPhS$)_2Cp_2$ (2b). A solution of **1** (235 mg, 0.463 mmol) and diphenylacetylene (258 mg, 1.45 mmol) in CH_2Cl_2 (40 mL) was heated to reflux for 24 h. After rotary evaporation of the solvent, chromatography of the residue gave **2b** (240 mg, 64%) as a green-brown band eluted slowly with light petroleum/CH_2Cl_2 (1:1) changing progressively to pure CH_2Cl_2.

2b: mp >300 °C. ^1H NMR: δ 7.11−6.83 (m, 20 H, Ph), 6.05 (s, 10 H, Cp). Found: C, 49.19; H, 3.47; S, 14.32. Anal. Calcd for $C_{38}H_{30}Mo_2S_4{\cdot}2CH_2Cl_2$: C, 49.13; H, 3.48; S, 13.10. MS: *m*/*z* 807 (M^+).

Synthesis of *cis*- and *trans*-$Mo_2\{\mu$-SCH=C(CO$_2$Me)S$\}Cp_2$ (2c). A solution of complex **1** (504 mg, 0.995 mmol) and methyl propiolate (1.2 mL) in CH_2Cl_2 (40 mL) was refluxed for 24 h. Separation of the products by chromatography gave two bands: the orange-red trans isomer (152 mg, 25%) was eluted first with light petroleum/CH_2Cl_2 (1:4), followed by a yellow band of the more polar cis isomer (236 mg, 37%), which was eluted with acetone/CH_2Cl_2 (1:99). Crystals of the trans isomer suitable for X-ray analysis were grown by diffusion from CH_2Cl_2 and diethyl ether.

cis-**2c**: mp >300 °C. ^1H NMR: δ 7.78 (s, 2 H, CH), 6.13 (s, 10 H, Cp), 3.55 (s, 6 H, Me). Found: C, 34.92; H, 2.99; S, 20.63.

(33) Cowans, B.; Rakowski Dubois, M. In *Organometallic Syntheses*; King, R. B., Ed.; Elsevier: Amsterdam, 1986; Vol. 3, p 262.
(34) Bruce, M. I.; Hameister, C.; Swincer, A. G. *Inorg. Synth.* **1990**, *28*, 270.
(35) Hallman, P. S.; Stephenson, T. A.; Wilkinson, G. *Inorg. Synth.* **1970**, *12*, 237.
(36) Morris, M. J.; Precious, G., unpublished work.
(37) Connelly, N. G.; Geiger, W. E. *Chem. Rev.* **1996**, *96*, 877. In this review, the potential of the ferrocenium/ferrocene couple is given as 0.46 V vs SCE, which equates to 0.505 V vs AgCl/Ag, rather than the 0.55 V which we observed. No correction to the observed potentials has been made for this discrepancy.

Anal. Calcd for $C_{18}H_{18}Mo_2O_4S_4$: C, 34.96; H, 2.93; S, 20.74. MS: *m*/*z* 618 (M^+).

trans-**2c**: mp >300 °C. ^{1}H NMR: δ 7.80 (s, 2 H, CH), 6.13 (s, 10 H, Cp), 3.55 (s, 6 H, Me). ^{13}C NMR: δ 163.3 (CO_2Me), 162.0 (CH), 159.2 (CCO_2Me), 97.0 (Cp), 52.2 (Me). Found: C, 35.18; H, 2.87; S, 20.68. Anal. Calcd for $C_{18}H_{18}Mo_2O_4S_4$: C, 34.96; H, 2.93; S, 20.74%. MS: *m*/*z* 618 (M^+).

Synthesis of $Mo_2\{\mu$-SC(CO_2Me)=C(CO_2Me)S$\}(\mu$-SCH_2CH_2S)-Cp_2 (3a). A solution of $Mo_2(\mu$-$SCH_2CH_2S)_2Cp_2$ (500 mg, 0.988 mmol) and 1 equiv of DMAD (0.121 mL) in CH_2Cl_2 (30 mL) was stirred for 4 days. The solvent was removed, and the residue was chromatographed. Two bands were eluted with acetone−CH_2Cl_2 (1:99). The first, apple green in color, contained the monodithiolene complex **3a** (271 mg, 44%), and the second (red) consisted of bis-dithiolene complex **2a** (199 mg, 27% yield based on Mo). The elemental analysis of **3a** consistently gave a high value for carbon but correct values for H and S (four attempts)

3a: mp, 164−168 °C. ^{1}H NMR: δ 5.58 (s, 10 H, Cp), 3.65 (s, 6 H, Me), 1.87 (s, 4 H, CH_2). ^{13}C NMR: δ 166.2 (CO_2Me), 164.2 (CCO_2Me), 93.4 (Cp), 52.5 (Me), 34.6 (CH_2). Found: C, 36.74; H, 3.44; S, 20.44. Anal. Calcd for $C_{18}H_{20}Mo_2O_4S_4$: C, 34.84; H, 3.25; S, 20.67. MS: *m*/*z* 620 (M^+), 592 ($M^+ - C_2H_4$), 450, 418, 386 ($Mo_2S_{4-n}Cp_2^+$, $n = 0-2$).

Synthesis of $Mo_2(\mu$-SCPh=CPhS$)(\mu$-$SCH_2CH_2S)Cp_2$ (3b). In a similar manner, a solution of **1** (505 mg, 1.003 mmol) and 1 equiv of diphenylacetylene (178 mg) in CH_2Cl_2 (40 mL) was stirred for 5 days. Column chromatography of the mixture gave a light green band of **2b** (30 mg, 3.7% based on Mo), eluted with CH_2Cl_2−light petroleum (1:1). Further elution with a 3:2 mixture of the same solvents developed a darker green band due to **3b** (131 mg, 20% yield).

3b: mp >300 °C. ^{1}H NMR: δ 7.15−6.90 (m, 10 H, Ph), 5.55 (s, 10 H, Cp), 1.85 (s, 4 H, CH_2). ^{13}C NMR: δ 157.4 (CPh), 138.0 (C_{ipso}), 127.9−127.2 (m, Ph), 92.5 (Cp), 34.7 (CH_2). Found: C, 48.35; H, 3.67; S, 19.36. Anal. Calcd for $C_{26}H_{24}Mo_2S_4$: C, 47.60; H, 3.69; S, 19.55. MS: *m*/*z* 628 ($M^+ - C_2H_4$), 450, 418, 386 ($Mo_2S_{4-n}Cp_2^+$, $n = 0-2$).

Synthesis of $Mo_2\{\mu$-SC(CO_2Me)=C(CO_2Me)S$\}(\mu$-SCPh=CPhS$)Cp_2$ (2d). A solution of $Mo_2\{\mu$-SC(CO_2Me)=C(CO_2Me)S$\}$-$(\mu$-$SCH_2CH_2S)Cp_2$ (**3a**) (202 mg, 0.326 mmol) and diphenylacetylene (55 mg, 0.31 mmol) in CH_2Cl_2 (30 mL) was heated to reflux for 24 h, after which time the solvent was removed. Column chromatography gave a single yellow-brown band consisting of **2d** (207 mg, 83%) eluted in CH_2Cl_2. Red plates suitable for X-ray analysis were grown from toluene solution.

2d: mp >300 °C. ^{1}H NMR: δ 7.10−6.77 (m, 10 H, Ph), 6.23 (s, 10 H, Cp), 3.63 (s, 6 H, Me). ^{13}C NMR: δ 166.1 (CO_2Me), 161.3 (CCO_2Me), 153.3 (CPh), 137.8 (C_{ipso}), 128.1−126.8 (m, Ph), 96.6 (Cp), 52.6 (Me). Found: C, 46.66; H, 3.32; S, 16.62. Anal. Calcd for $C_{30}H_{26}Mo_2O_4S_4$: C, 46.67; H, 3.40; S, 16.64. MS: *m*/*z* 772 (M^+).

Synthesis of $Mo_2\{\mu$-SC(CO_2Me)=C(CO_2Me)S$\}\{\mu$-SCH=C-(CO_2Me)S$\}Cp_2$ (2e). A solution of $Mo_2\{\mu$-SC(CO_2Me)=C(CO_2-Me)S$\}(\mu$-$SCH_2CH_2S)Cp_2$ (**3a**) (133 mg, 0.215 mmol) and methyl propiolate (0.038 mL) in CH_2Cl_2 (30 mL) was heated to reflux for 24 h. Column chromatography gave one yellow-brown band, consisting of **2e** (72 mg, 50%), which was eluted with acetone-CH_2Cl_2 (1:99).

2e: mp, 244 °C. ^{1}H NMR: δ 7.78 (s, 1 H, CH), 6.17 (s, 10 H, Cp), 3.59 (s, 6 H, co-incident Me), 3.56 (s, 3H, Me). ^{13}C NMR: δ 166.0, 165.4, 163.2 (all *C*O_2Me), 161.5 (CH), 161.5, 159.7, 158.1 (all *C*CO_2Me), 97.3 (Cp), 52.5 (2 Me), 52.3 (Me). Found: C, 35.48; H, 2.77; S, 18.93. Anal. Calcd for $C_{20}H_{20}Mo_2O_6S_4$: C, 35.51; H, 2.98; S, 18.96. MS: *m*/*z* 676 (M^+).

Synthesis of $Mo_2\{\mu$-SCH=C(CO_2Me)S$\}(\mu$-SCPh=CPhS$)Cp_2$ (2f). A solution of **3b** (140 mg, 0.213 mmol) and methyl propiolate (0.04 mL) in CH_2Cl_2 (30 mL) was heated to reflux for 24 h. Column chromatography gave one orange-yellow band, consisting of **2f** (106 mg, 70%), which was eluted with CH_2Cl_2.

2f: mp, dec above 250 °C. ^{1}H NMR: δ 7.82 (s, 1 H, CH), 7.15−6.76 (m, 10 H, Ph), 6.07 (s, 10 H, Cp), 3.58 (s, 3 H, Me). ^{13}C NMR: δ 163.6 (*C*O_2Me), 163.2 (CH), 158.9 (*C*CO_2Me), 154.3, 153.5 (CPh), 138.0, 137.9 (C_{ipso}), 128.0−126.7 (m, Ph), 96.1 (Cp), 52.2 (Me). Found: C, 47.26; H, 3.39; S, 18.12. Anal. Calcd for $C_{28}H_{24}Mo_2O_2S_4$: C, 47.19; H, 3.39; S, 18.00. MS: *m*/*z* 712 (M^+).

Synthesis of $Mo_2\{\mu$-SC(CO_2Me)=C(CO_2Me)S$\}\{\mu$-SC(PPh_2)=C(PPh_2)S$\}Cp_2$ (2g). A solution of **3a** (385 mg, 0.637 mmol) and dppa (376 mg, 0.95 mmol) in CH_2Cl_2 (30 mL) was heated to reflux for 24 h. Column chromatography produced one orange-yellow band, eluted with CH_2Cl_2, consisting of **2g** (392 mg, 62%). Crystals suitable for X-ray analysis were grown by diffusion from CH_2Cl_2 and diethyl ether.

2g: mp, 230−232 °C. ^{1}H NMR: δ 7.42−7.16 (m, 20 H, Ph), 5.57 (s, 10 H, Cp), 3.54 (s, 6 H, Me). ^{13}C NMR: δ 173.4 (d of d, J = 1.5, 3.8 Hz, *C*PPh_2), 165.7 (CO_2Me), 161.1 (*C*CO_2Me), 135.3 (apparent t, C_{ipso}), 133.0−128.9 (m, Ph), 96.4 (Cp), 52.4 (Me). ^{31}P NMR: δ −10.1. Found: C, 48.27; H, 3.36; S, 12.82. Anal. Calcd for $C_{42}H_{36}Mo_2O_4P_2S_4 \cdot CH_2Cl_2$: C, 48.19; H, 3.57; S, 11.97. MS: *m*/*z* 987 (M^+).

Synthesis of $Mo_2\{\mu$-SC(PPh_2)=C(PPh_2)S$\}_2Cp_2$ (2h). The phosphine $Ph_2PC{\equiv}CPPh_2$ (522 mg, 1.32 mmol) was added to a solution of **1** (295 mg, 0.583 mmol) in CH_2Cl_2 (40 mL), which was then refluxed for 48 h. Column chromatography produced two small unidentified yellow bands, followed by an orange-yellow zone due to complex **2h**. The yield was 273 mg, 38%. The compound proved too insoluble for the recording of a ^{13}C NMR spectrum. Crystals suitable for X-ray analysis were grown by diffusion from CH_2Cl_2 and diethyl ether.

2h: mp, dec above 280 °C. ^{1}H NMR: δ 7.42−7.16 (m, 40 H, Ph), 4.87 (s, 10 H, Cp). ^{31}P NMR: δ −9.1. Found: C, 59.49; H, 3.96; S, 10.30. Anal. Calcd for $C_{62}H_{50}Mo_2P_4S_4$: C, 60.09; H, 4.07; S, 10.35. MS: *m*/*z* 1238 (M^+).

Preparation of $Mo_2\{\mu$-SC(PPh_2)=C(PPh_2)S$\}(\mu$-$SCH_2CH_2S)$-Cp_2 (3c). A solution of complex **1** (529 mg, 1.045 mmol) and dppa (412 mg, 1.045 mmol) in CH_2Cl_2 was stirred at room temperature for 5 days. Column chromatography gave a small unidentified yellow band followed by a light green band of **3c** (175 mg, 19%) eluted with CH_2Cl_2−light petroleum (7:3). Two further bands were obtained on elution with CH_2Cl_2 but could not be identified.

3c: mp, dec above 225 °C. ^{1}H NMR: δ 7.45−7.15 (m, 20 H, Ph), 4.97 (s, 10 H, Cp), 1.67 (s, 4 H, CH_2). ^{13}C NMR: δ 177.9 (d, J = 2.3 Hz, $CPPh_2$), 135.9 (apparent t, C_{ipso}), 133.1−128.1 (m, Ph), 92.3 (Cp), 34.4 (CH_2). ^{31}P NMR: δ −9.3. Found: C, 52.42; H, 3.79; S, 14.49. Anal. Calcd for $C_{38}H_{34}Mo_2P_2S_4$: C, 52.29; H, 3.93; S, 14.70. MS: *m*/*z* 873 (M^+).

Synthesis of $Mo_2\{\mu$-SC(CO_2Me)=C(CO_2Me)S$\}\{\mu$-SC(PPh_2)=C(PPh_2)S$\}Cp_2$(RuClCp) (4a). Complex **2g** (116.2 mg, 0.118 mmol) and $CpRu(PPh_3)_2Cl$ (95.1 mg, 0.131 mmol) were dissolved in toluene (50 cm^3). The solution was heated to reflux for 5 h, after which the solvent was removed and the residue absorbed on silica. Column chromatography produced one orange-brown band of **4a** (104.2 mg, 74% yield based on Mo), which was eluted with CH_2Cl_2−acetone (99:1).

4a: mp >300 °C. ^{1}H NMR: δ 7.65−6.94 (m, 20H, Ph), 6.03, 5.58 (s, 5H, MoCp), 4.42 (s, 5H, RuCp), 3.55 (s, 6H, CO_2Me). ^{13}C

Table 4. Summary of Crystallographic Data for the Six Structures

	trans-**2c**	**2d**·C_6H_5Me
empirical formula	$C_{18}H_{18}Mo_2O_4S_4$	$C_{37}H_{34}Mo_2O_4S_4$
fw	618.44	862.76
cryst syst	monoclinic	triclinic
space group	$P2_1/c$	$P\bar{1}$
a/Å	9.2537(7)	8.141(1)
b/Å	9.4933(7)	15.020(2)
c/Å	11.8024(9)	15.855(2)
α/deg	90	111.491(3)
β/deg	98.249(1)	91.397(3)
γ/deg	90	101.413(3)
V/Å^3	1026.1(1)	1758.3(4)
Z	2	2
θ range for data collection/deg	2.22−28.32	1.49−28.29
reflns collected	6260	10 889
independent reflns	2461 [*R*(int) = 0.0889]	7947 [*R*(int) = 0.0868]
data/restraints/params	2461/0/127	7947/30/424
GOF on F^2	1.157	0.926
final R1, wR2 [$I > 2\sigma(I)$]	R1 = 0.0525, wR2 = 0.1230	R1 = 0.0642, wR2 = 0.1489
(all data)	R1 = 0.0602, wR2 = 0.1288	R1 = 0.1126, wR2 = 0.1701
largest diff peak and hole/e·Å^{-3}	1.177 and −3.820	2.579 and −2.342

	2g·CH_2Cl_2	**2h**
empirical formula	$C_{43}H_{38}Cl_2Mo_2O_4P_2S_4$	$C_{62}H_{50}Mo_2P_4S_4$
fw	1071.69	1239.02
cryst syst	orthorhombic	monoclinic
space group	$P2_12_12_1$	$P2_1/n$
a/Å	10.484(3)	14.475(5)
b/Å	17.491(4)	10.517(4)
c/Å	23.751(6)	18.194(6)
α/deg	90.000(6)	90
β/deg	90.000(6)	105.430(7)
γ/deg	90.000(6)	90
V/Å^3	4355(2)	2670(2)
Z	4	2
θ range for data collection/deg	1.45−28.32	1.61−25.00
reflns collected	27 108	13 021
independent reflns	10 491 [*R*(int) = 0.0861]	4690 [*R*(int) = 0.0857]
data/restraints/params	10491/311/524	4690/239/325
GOF on F^2	0.881	0.969
final R1, wR2 [$I > 2\sigma(I)$]	R1 = 0.0491, wR2 = 0.0742	R1 = 0.0501, wR2 = 0.0895
(all data)	R1 = 0.0880, wR2 = 0.0827	R1 = 0.1019, wR2 = 0.1022
largest diff peak and hole/e·Å^{-3}	0.905 and −1.020	0.859 and −1.081

	4a	*syn*-**4b**·$2CH_2Cl_2$
empirical formula	$C_{47}H_{41}ClMo_2O_4P_2RuS_4$	$C_{74}H_{64}Cl_6Mo_2P_4Ru_2S_4$
fw	1188.38	1812.09
cryst syst	orthorhombic	monoclinic
space group	$P2_12_12_1$	$P2_1/c$
a/Å	10.525(3)	19.551(5)
b/Å	14.839(4)	19.742(5)
c/Å	29.328(8)	21.079(6)
α/deg	90	90
β/deg	90	116.572(5)
γ/deg	90	90
V/Å^3	4580(2)	7277(3)
Z	4	4
θ range for data collection/deg	1.54−28.32	1.16−28.29
reflns collected	23 503	45 612
independent reflns	10 562 [*R*(int) = 0.0806]	17 552 [*R*(int) = 0.0856]
data/restraints/params	10562/342/550	17552/570/836
GOF on F^2	1.058	0.928
final R1, wR2 [$I > 2\sigma(I)$]	R1 = 0.0359, wR2 = 0.0849	R1 = 0.0633, wR2 = 0.1516
(all data)	R1 = 0.0406, wR2 = 0.0872	R1 = 0.1143, wR2 = 0.1694
largest diff peak and hole/e·Å^{-3}	1.366 and −0.934	2.164 and −1.753

NMR: δ 181.8 (d of d, J = 34.3 and 34.3 Hz, *C*PPh_2), 165.2 (*C*O_2-Me), 160.2 (*C*CO_2Me), 136.5, 132.2 (apparent d of t, C_{ipso}, Ph), 133.9, 132.1, 127.5, 126.7 (apparent t, Ph), 129.7, 129.3 (Ph), 97.4, 96.6 (MoCp), 79.1 (RuCp), 52.2 (Me). ^{31}P NMR: δ 60.8. Found: C, 47.62; H, 3.27; Cl, 3.06; S, 10.62. Anal. Calcd for $C_{47}H_{41}ClMo_2O_4P_2RuS_4$: C, 47.46; H, 3.47; Cl, 2.98; S, 10.78. MS: *m*/*z* 1190 (M^+).

Synthesis of $Mo_2\{\mu$-SC(PPh$_2$)=C(PPh$_2$)S$\}_2$Cp$_2$(RuClCp)$_2$ (4b). A solution of **2h** (251 mg, 0.203 mmol) and $CpRu(PPh_3)_2Cl$ (320 mg, 0.441 mmol) in toluene (50 cm^3) was refluxed for 6 h, then absorbed onto silica and chromatographed. Elution with CH_2Cl_2−acetone (99:1) developed two minor pale yellow bands which were discarded, followed by an orange band and a red band. The orange band consisted of the anti isomer of **4b** (40.8 mg, 12.3% based on

Mo), and the red band consisted of the syn isomer (128.1 mg, 38.5% based on Mo); the latter was washed with diethyl ether to remove a small amount of a green impurity. The former complex proved too insoluble to obtain a ^{13}C NMR spectrum.

anti-**4b**: mp >300 °C. ^1H NMR: δ 7.64−6.85 (m, 40H, Ph), 5.38 (s, 10H, MoCp), 4.35 (s, 10H, RuCp). ^{31}P NMR: δ 61.3. Found: C, 52.73; H, 3.60; Cl, 4.52; S, 8.03. Anal. Calcd for $C_{72}H_{60}Cl_2Mo_2P_4Ru_2S_4$: C, 52.66; H, 3.68; Cl, 4.32; S, 7.81. MS: *m*/*z* 1643 ($M + H^+$).

syn-**4b**: mp >300 °C. ^1H NMR: δ 7.62−6.90 (m, 40H, Ph), 5.77, 4.87 (both s, 5H, MoCp), 4.36 (s, 10H, RuCp). ^{13}C NMR: δ 182.5 (d of d, J = 34.7 and 34.7 Hz, *C*PPh_2), 137.1−127.0 (m, Ph), 96.9, 95.7 (MoCp), 79.5 (RuCp). ^{31}P NMR: δ 61.7. Found: C, 52.51; H, 3.51; Cl, 4.38; S, 7.78. Anal. Calcd for $C_{72}H_{60}Cl_2Mo_2P_4Ru_2S_4$: C, 52.66; H, 3.68; Cl, 4.32; S, 7.81. MS: *m*/*z* 1642 (M^+).

Synthesis of $RuCl_2\{Mo_2\{\mu$-SC(CO$_2$Me)=C(CO$_2$Me)S$\}\{\mu$-SC(PPh$_2$)=C(PPh$_2$)S$\}$Cp$_2\}_2$ (5). A solution containing $RuCl_2(PPh_3)_3$ (100 mg, 0.104 mmol) in acetone (40 mL) was treated with solid **2g** (206 mg, 0.208 mmol) and then stirred for 2 h. The insoluble orange-beige product **5** (80 mg, 36%) was then filtered off and washed with acetone.

5: mp >300 °C. Found: C, 46.77; H, 3.50; Cl, 3.37; S, 11.62. Anal. Calcd for $C_{84}H_{72}Cl_2Mo_4O_8P_4RuS_8$: C, 47.02; H, 3.38; Cl, 3.30; S, 11.96. Electrospray MS: *m*/*z* 2147 (M^+).

Crystal Structure Determinations. The crystal data for the six structures (*trans*-**2c**, **2d**, **2g**, **2h**, **4a**, and *syn*-**4b**) are collected in Table 4. General procedures were as described in previous publications. A Bruker Smart CCD area detector with Oxford Cryosystems low-temperature system was used for data collection at 150(2) K. Complex scattering factors were taken from the program package *SHELXTL*[38] as implemented on a Viglen Pentium computer. Hydrogen atoms were placed geometrically and refined in riding mode with U_{iso} constrained to be 1.2 times U_{eq} of the carrier atom.

Calculations. DFT calculations utilized the *Gaussian 03W* program (revision C.02).[39] The spin-restricted method modeled the closed-shell species, and the spin-unrestricted method modeled the open-shell species. The geometries of the crystal structures, where available, were used to derive percent composition of the frontier molecular orbitals using the B3LYP exchange-correlation functional[40,41] with the LanL2DZ basis set.[42−45] Tight SCF convergence (10−8 a.u.) was used for all calculations. TD-DFT[46−48] was used to calculate the energies and intensities of the 35−50 lowest-energy electronic transitions of each complex (15 for the large oxidized **4a** and **4b** species). These were transformed with the *SWizard* program[49] into simulated spectra as described before,[50] using Gaussian functions with half-widths of 3000 cm^{-1}. For comparison purposes and to derive data for the oxidized species, the DFT-geometry-optimized structures were obtained for species **4a** and its oxidized product $\mathbf{4a}^+$ ($S = {}^1/_2$) and also for $\mathbf{4b}^+$ ($S = {}^1/_2$), $\mathbf{4b}^{2+}$ ($S = 0$) and $\mathbf{4b}^{3+}$ ($S = {}^1/_2$).

Molecular orbital compositions and the overlap populations were calculated using the *AOMix* program[51] using the Mulliken scheme.[52−54] Atomic charges were calculated using the Mulliken procedure as implemented in *Gaussian 03*.

Acknowledgment. This work was supported by the EPSRC (studentship to A.E.R.), the University of Sheffield, and the Natural Sciences and Engineering Research Council (Ottawa) (ABPL). We also thank Johnson Matthey for a generous loan of ruthenium chloride, Prof. M.D. Ward for useful discussions, and Drs. D. Collison and J. Wolowska (University of Manchester) for recording and simulating the EPR spectra.

Supporting Information Available: CIF files for the six crystal structures, observed and calculated isotope patterns for the molecular ion in the mass spectrum of complex **5**, and more detailed DFT results in Tables S1−S2. This material is available free of charge via the Internet at http://pubs.acs.org.

IC701201X

(38) Sheldrick, G. M. *SHELXTL, An Integrated System for Solving, Refining and Displaying Crystal Structures from Diffraction Data*, revision 5.1; Bruker AXS, Ltd.: Madison, WI, 1997.

(39) Frisch, M. J.; Trucks, G. W.; Schlegel, H. B.; Scuseria, G. E.; Robb, M. A.; Cheeseman, J. R.; Montgomery, J. A., Jr.; Vreven, T.; Kudin, K. N.; Burant, J. C.; Millam, J. M.; Iyengar, S. S.; Tomasi, J.; Barone, V.; Mennucci, B.; Cossi, M.; Scalmani, G.; Rega, N.; Petersson, G. A.; Nakatsuji, H.; Hada, M.; Ehara, M.; Toyota, K.; Fukuda, R.; Hasegawa, J.; Ishida, M.; Nakajima, T.; Honda, Y.; Kitao, O.; Nakai, H.; Klene, M.; Li, X.; Knox, J. E.; Hratchian, H. P.; Cross, J. B.; Bakken, V.; Adamo, C.; Jaramillo, J.; Gomperts, R.; Stratmann, R. E.; Yazyev, O.; Austin, A. J.; Cammi, R.; Pomelli, C.; Ochterski, J. W.; Ayala, P. Y.; Morokuma, K.; Voth, G. A.; Salvador, P.; Dannenberg, J. J.; Zakrzewski, V. G.; Dapprich, S.; Daniels, A. D.; Strain, M. C.; Farkas, O.; Malick, D. K.; Rabuck, A. D.; Raghavachari, K.; Foresman, J. B.; Ortiz, J. V.; Cui, Q.; Baboul, A. G.; Clifford, S.; Cioslowski, J.; Stefanov, B. B.; Liu, G.; Liashenko, A.; Piskorz, P.; Komaromi, I.; Martin, R. L.; Fox, D. J.; Keith, T.; Al-Laham, M. A.; Peng, C. Y.; Nanayakkara, A.; Challacombe, M.; Gill, P. M. W.; Johnson, B.; Chen, W.; Wong, M. W.; Gonzalez, C.; Pople, J. A. *Gaussian 03*, revision C.02; Gaussian, Inc.: Wallingsford, CT, 2004.

(40) Lee, C.; Yang, W.; Parr, R. G. *Phys. Rev. B: Condens. Matter Mater. Phys.* **1988**, *37*, 785.

(41) Becke, A. D. *J. Chem. Phys.* **1993**, *98*, 5648.

(42) Dunning, T. H., Jr.; Hay, P. J. In *Modern Theoretical Chemistry*; Schaefer, H. F. I., Ed.; Plenum: New York, 1976; Vol. 3, p 1.

(43) Hay, P. J.; Wadt, W. R. *J. Chem. Phys.* **1985**, *82*, 270.

(44) Hay, P. J.; Wadt, W. R. *J. Chem. Phys.* **1985**, *82*, 284.

(45) Hay, P. J.; Wadt, W. R. *J. Chem. Phys.* **1985**, *82*, 299.

(46) Stratmann, R. E.; Scuseria, G. E.; Frisch, M. J. *J. Chem. Phys.* **1998**, *109*, 8218.

(47) Bauernschmitt, R.; Ahlrichs, R. *Chem. Phys. Lett.* **1996**, *256*, 454.

(48) Casida, M. E.; Jamorski, C.; Casida, K. C.; Salahub, D. R. *J. Chem. Phys.* **1998**, *108*, 4439.

(49) Gorelsky, S. I. *SWizard* program, revision 4.2. http://www.sg-chem.net/swizard/.

(50) Gorelsky, S. I. In *Comprehensive Coordination Chemistry-II;* McCleverty, J. A., Meyer, T. J., Eds.: Elsevier Pergamon: New York, 2003; Vol. 2, Chapter 2.51, pp 651.

(51) Gorelsky, S. I. *AOMix: Program for Molecular Orbital Analysis*; York University: Toronto, 1997. http://www.sg-chem.net/.

(52) Mulliken, R. S. *J. Chem. Phys.* **1955**, *23*, 2338.

(53) Mulliken, R. S. *J. Chem. Phys.* **1955**, *23*, 1833.

(54) Mulliken, R. S. *J. Chem. Phys.* **1955**, *23*, 2343.

(55) Mulliken, R. S. *J. Chem. Phys.* **1955**, *23*, 1841.